Millimeter-Wave Channel Modeling in a VANETs using Coding Techniques

Arshee Ahmed[1]**, Haroon Rasheed**[1]**, Ali Kashif Bashir**[2,3]**, and Marwan Omar**[4]

[1]*****Electrical Engineering, Bahria University, Karachi, Pakistan.**
[2]**Department of Computing and Mathematics, Manchester Metropolitan University, Manchester, United Kingdom**
[3]**School of Business, Woxsen University, India**
[4]**Department of Information Technology and Management, Illinois Institute of Technology, USA**

Corresponding author:
Arshee Ahmed[1]

Email address: 02-281171-001@student.bahria.edu.pk

ABSTRACT

Vehicular ad-Hoc Network (VANET) is envisioned to ensure wireless transmission with ultra-high reliability. In the presence of fading and mobility of vehicles, error-free information between Vehicle to Vehicle (V2V) and Vehicle to Infrastructure (V2I) requires extensive investigation. The current literature lacks in designing an ultra-reliable comprehensive tractable model for VANET using millimeter wave. Ultra-reliable communication is needed to support autonomous vehicular communication. This article aims to provide a comprehensive tractable model for Vehicular ad-Hoc Network (VANET) over millimeter waves using Space-Time-Block-Coding (STBC) concatenated with Reed Solomon (RS) coding. The designed model provides the fastest way of designing and analyzing VANET networks on 60 GHz. By using the derived BER expressions and Reed Solomon coded Doppler expression ultra-reliable vehicular networks can be build meeting the demands of massive growing volume of traffic. The performance of the model is compared with previous BER computational techniques and existing VANET communication systems, i.e. IEEE 802.11bd and 3rd Generation Partnership Project Vehicle to Everything (3GPP V2X). The findings show that our proposed approach outperforms IEEE 802.11bd and the results are comparable with V2X NR. Packet Error Rate (PER), Packet Reception Ratio (PRR) and throughput are used as performance metrics. We have also evaluated the model on higher velocities of vehicles. Further, the simulation and numerical findings show that the proposed system surpass the existing BER results comprising of various modulation and coding techniques. The simulation results are verified by the numerical results there-by, showing the accuracy of our derived expressions.

INTRODUCTION

In recent years, there has been significant demand for communication in Vehicular ad-Hoc Network (VANET) at high data rates. To meet the enormous communication demand in VANET, it is necessary to utilize the scarce resources, such as power and bandwidth, as effectively as feasible. Reliability, throughput, and accuracy are significant factors because of multipath fading and the rapid mobility of vehicle nodes. VANET communication system is susceptible to a certain level of noise, shadowing and fading. The Line of Sight (LOS) obstruction by vehicles results in an extra loss of the received power of approximately 10 dB (abbas2015measurement). In (va2016millimeter) atmospheric attenuation at 60 GHz is studied for number of vehicles, which is 15dB/km and excessive path loss of 30 dB occurs for three obstructing vehicles. Analytical research on a Markov chain model is used in VANETs to examine the impact of channel fading on IEEE 802.11p. The performance is evaluated on Nakagami-m, Rayleigh, and Rician fading channels using BER (shah2022influence). Highly mobile vehicular nodes and rapidly changing network topology throws many challenges in the dissemination of critical messages in VANET (giripunje2022routing). Furthermore, the multipath propagation also leads to signal distortion

47 and burst errors. Therefore, transmission reliability is very challenging in wireless channels. Forward
48 Error Correction (FEC) is one of the most commonly used techniques to provide reliable communication.
49 The new Task Group TGbd was recently formed with the goal of exploring the future road map for Vehicle
50 to Everything (V2X) and working towards a new standard known as Next-Generation V2X (NGV).
51 802.11bd is an 802.11p modification that specifies changes to the IEEE 802.11 Medium Access Control
52 (MAC) and Physical Layer (PHY) layers for V2X communications in the 5.9 GHz and 60 GHz frequency
53 bands. Currently, millimeter-wave (mmWave) massive Multi-Input Multi-Output (MIMO) is the most
54 potential technology for vehicular communication (yi2020novel). The mmWave signals are susceptible to
55 high free-space path loss caused by high atmospheric attenuation (shen2019channel).
56 Beamforming techniques are used in mmWave systems to mitigate the effects of large path losses by
57 providing enough channel space (kutty2015beamforming). The traditional MIMO system performance is
58 enhanced due to multiple antennas systems at both links end. Thus providing an effective solution for
59 future wireless communications systems as they provide high data rates. Beamforming signal processing
60 techniques enable transmission and reception in the needed directions by applying appropriate antenna
61 port phases and amplitudes by using what is known as the "weighting approach". An adaptive algorithm
62 instantly calculates the complex weights w_k to steer the null antenna pattern toward competing signals
63 and the maximum antenna radiation pattern toward the chosen vehicular node.
64 In this research work, a VANET architecture is proposed using concatenated Space Time Block Coding -
65 Reed Solomon (STBC-RS) coding in which the reliability of VANET communication is targeted. Error
66 control coding technique using mmWave for minimizing errors is still a topic for rigorous investigation.
67 Currently for ITS 5G communication, ultra-reliable networks are required meeting the demands of 1- 10^{-5}
68 as indicated in (ghafoor2020millimeter). Moreover autonomous vehicles require reliable connectivity 1-
69 10^{-7} (schulz2017latency).
70
71
72 Rayleigh fading channel is used in the proposed approach to model the fading characteristics of the
73 channel. Because signal amplitude follow Rayleigh distribution when the line of sight (LOS) component
74 gradually diminishes in Vehicle to Vehicle (V2V) communication. Rayleigh fading is most suitable in
75 congested city roads, as concluded as a result of extensive simulations (jameel2017performance).

Contributions

77 The main contributions of this study are as follows:

78 • An ultra-reliable manipulable mathematical model is presented using RS coding along with 4*4
79   STBC. Transmit beamforming is employed by a complex weight expression of beamforming in the
80   model.

81 • Two closed-form expressions for RS coding in the AWGN channel and in Rayleigh fading are
82   derived. The numerical and simulation results have been obtained, which also verify our theoretical
83   formulations.

84 • The results show that AWGN BER approximation outperforms conventional 64-QAM and M-PSK
85   systems.

86 • The results also show that the proposed approach outmatched previous BER conputation ap-
87   proaches i.e, (al2017enhancing), (mergu2016performance) ,(Tiwari2013BERPO), (indoonun-
88   don2021overview) , (saleh2019improving), (hajiyat2019channel) , (hamarsheh2022robust) shown
89   in results and discussion section.

90 • The performance of the proposed model is compared with IEEE 802.11bd and V2X NR. The Packet
91   Error Probability (PEP), throughput and Packet Reception Ratio (PRR) are used as performance
92   metrics. The results are compared in Table 4, Table 5 and Table 6. On comparing, it can be
93   remarked that the proposed model outperforms IEEE 802.11bd. For designing V2X architectures
94   RS error control coding performs better.

95 • MIMO-STBC along with RS can be used as a physical layer advancement technique in 802.11bd.

96 • We have also evaluated our results on higher velocities, achieving the BER of 10^{-6} to 10^{-7}. Atlast
97   the designed model is meeting the demands of ultra-reliability i.e 1- 10^{-5} which is .99999.

RELATED WORK

In (abuqamar2021stbc) STBC was combined with Orthogonal Frequency Division Multiplexing with Sub carrier-Power Modulation (OFDM-SPM) to analyze combination on a multi-path Rayleigh fading channel. BER and throughput were used as a performance metrics. It was concluded that using STBC the performance of original OFDM-SPM can be improved in terms of reliability. In ((indoonundon2021overview) to achieve ultra-reliable low latency communication in 5G, a detailed analysis of coding schemes was conducted. LDPC, polar codes, turbo codes were simulated using Quadrature Amplitude Modulation (16QAM) and 64QAM. In this work, lower BER is obtained on increasing modulation order M in QAM modulation. RS coding was used in Cooperative-Intelligent Transport System (C-ITS) communications. The performance was analyzed and compared with Wyner–Ash codes. The result showed RS code outperformed with Wyner–Ash codes. Our designed model and derivations can be used in various C-ITS communications (bocharova2019low). RS performance was evaluated using STBC-MIMO systems concatenated with M-ary Quadrature Amplitude Modulation (M-QAM) and M-ary Phase-Shift Keying (MPSK) ((mane2020evaluation). The performance of existing Cooperative MIMO (C-MIMO) was improved using C-MIMO-STBC (hai2021space). It has been proved that wireless link quality can be improved by MIMO STBC while keeping transmitted power or frequency bandwidth constant. The performance of IEEE 802.11p was improved by implementing Multiple Input Single-Output (MISO) with Orthogonal Frequency-Division Multiplexing (OFDM) system. The authors analyzed the impact of time-varying channel on the performance of Alamouti STBC in OFDM systems ((youssefi2020performance). 802.11p could not offer multi antenna communication. STBC-OFDM was used to analyze the performance of multi antennas. We have used STBC-RS channel model for improving reliability in VANET communication. In (triwinarko2021phy) LDPC along with Multi-Input Multi-Output-Space Time Block Coding (MIMO-STBC) was used to improve the physical layer of 802.11p. STBC was combined with Orthogonal Frequency Division Multiplexing with Sub carrier-Power Modulation (OFDM-SPM) to analyze combination on a multi-path Rayleigh fading channel. BER and throughput were used as a performance metrics. It was concluded that using STBC the performance of original OFDM-SPM can be improved in terms of reliability.

RS code was combined with Spatial Modulation (SM) and STBC along with cooperated source and relay (zhao2022optimized). Two closed-form approximations for BER Bose–Chaudhuri–Hocquenghem (BCH) coding and Alamouti Space Time Block Coding (BCH-ASTBC) were proposed for millimeter-wave VANET communication. The performance of conventional ASTBC equation was improved and the results were compared on different code rates (electronics10090992).

The performance of WDM using M-ary DPPM schemes was enhanced under Amplified Spontaneous Emission (ASE) noise effects, Interchannel Crosstalk (ICC), and Atmospheric Turbulence (AT) (elsayed2022performance). Due to multi-path fading and vehicle mobility, VANET communication is difficult in terms of reliability and throughput. The high mobility of vehicular communications, randomness in channel dynamics, and link interference are all significant challenges for vehicular networking. Many approaches have been investigated in this context to improve the efficiency of V2V and V2I communication. Researchers have expressed interest in using cooperative communications within vehicular networks to mitigate the impact of these challenges and improve reliability by allowing nodes to collaborate (ahmed2018cooperative). Spatial multiplexing MIMO was employed by modifying the existing IEEE 802.11p standard for high throughput. Spatial multiplexing MIMO supports real-time data transfer in a non-line-of-sight environment (dey2020high).

Cochannel interference degrades the system performance of mmWave radars mounted on vehicles. VANET-assisted interference mitigation approach was proposed that enables vehicles to coordinate their spectrum usage via multiple access. The proposed scheme was tested via a case study to show that the proposed scheme is useful in dense traffic with high mobility of vehicles (zhang2020vanet). MIMO systems are reliable and have high capacity. A beamformer transceiver design was proposed for the MIMO Orthogonal Frequency-Division Multiplexing (OFDM) system. It was used for highly reliable and spectrally efficient operation under the most damaging jamming attacks (jagannath2020high).

In (ali2019simulation) an architecture using massive MIMO was proposed. In the proposed architecture, vehicles are controlled using Global System Mobile (GSM) towers. GSM towers are equipped with 5G technology where towers can send and receive real-time information like the weather forecast, current temperature and city situation that comes under tower's control.

The diversity gain was obtained by the STBC in wireless communication. The basic idea of exploiting

153 transmit diversity was first developed by Vahid Tarokh and then a simpler structure was later introduced
154 by Alamouti. Later on, Almouti's work was extended and developed to originate space time block codes.
155 Full Duplex Non-Orthogonal Multiple Access (NOMA)-MIMO was employed in V2X systems and
156 closed-form approximations for ergodic capacity were derived (zhang2019performance). The transmis-
157 sion of multiple copies of data stream via the number of antennas can be achieved using Space-time block
158 codes MIMO. MIMO systems are used to improve data-transfer reliability by utilizing the various received
159 data versions. The decoding algorithm is simple in nature and accomplishes full diversity specified by
160 the number of transmit antennas at a radio receiver. STBC are complex and have same key features like
161 Alamouti. Further, their encoding and decoding schemes are also similar (santumon2012space). The
162 data stream is first encoded in blocks when using STBC. These data blocks are then distributed across
163 multiple antennas that are spaced apart. In (ehsanfar2022performance), the performance of three different
164 frame structures of IEEE 802.11p, IEEE 802.11bd-draft, and a Unique-Word (UW)-based physical layer
165 (PHY) were compared for vehicle-to-everything communication. Based on simulation results, it was
166 determined that the UW-based PHY achieved interference-free channel estimation performance using a
167 low complexity technique.
168 IEEE 802.11p does not perform well for high mobility networks. It uses Distributed Coordination Func-
169 tion (DCF) for communication between wireless nodes. In (hussain2017efficient), a RSU-based efficient
170 channel access scheme was proposed for VANETs under high traffic and mobility.

PROPOSED MODEL

172 A system model for VANET communication is described in Figure 1 in which V2V and Vehicle-to- Road
173 Side Unit (V2RSU) communication occurs. The sensors placed on vehicles receive information via four
174 receiving antennas. The received information is passed to the Data Fusion Unit which comprises of RS
175 and STBC, where the received information via multiple antennas is fused. The information is sent to
176 Distributed Processing Unit, where the data is processed and then it is transferred to other vehicle.
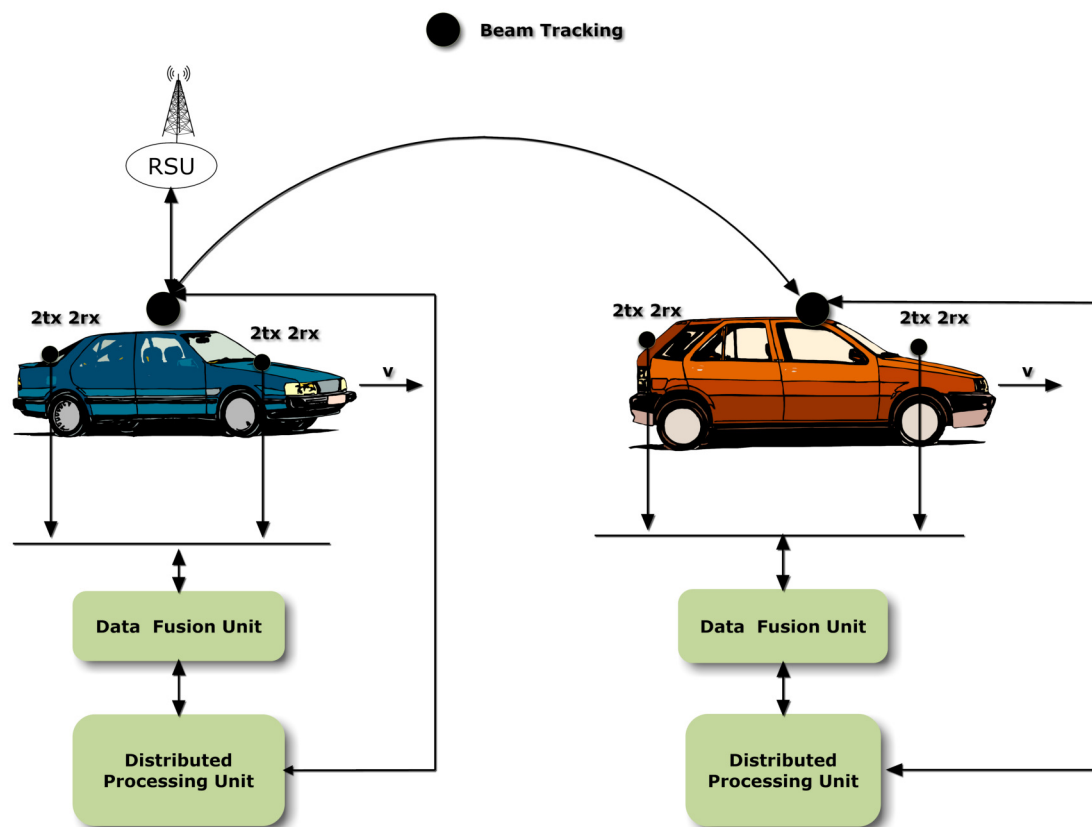
Figure 1. System Model for RS-STBC
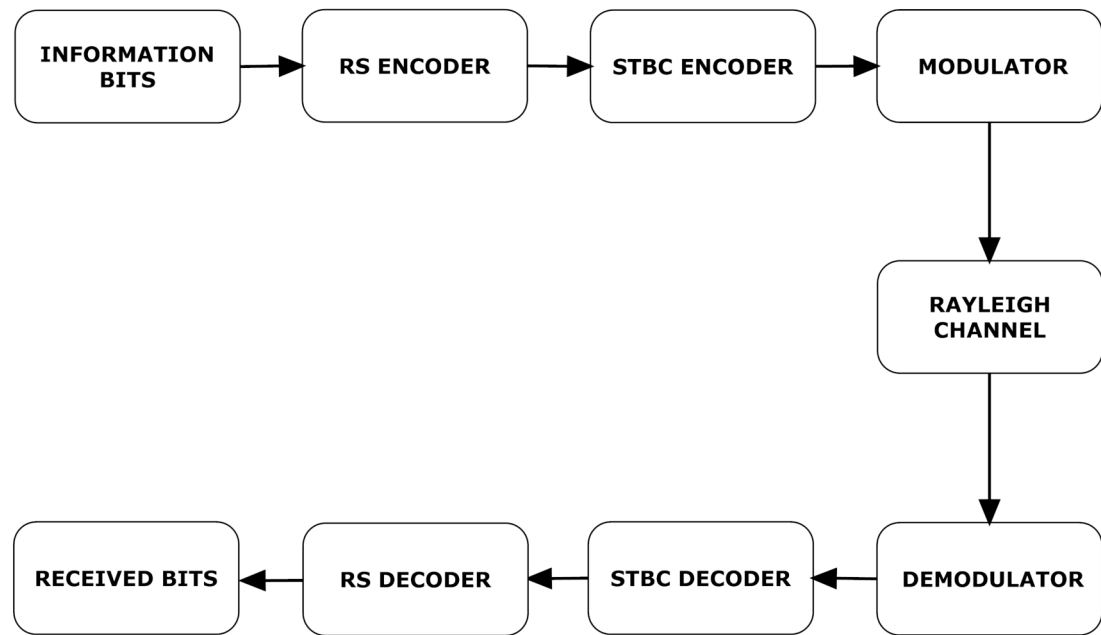
Figure 2. VANET Communication Process
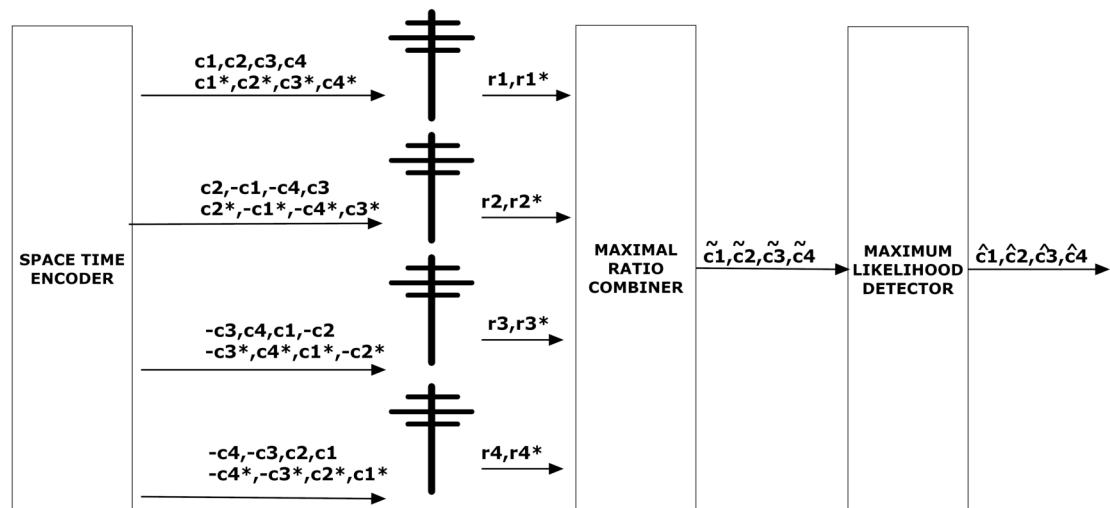
Figure 3. STBC Encoder and Decoder

177   A detailed communication process is illustrated in Figure 2. Information bits are encoded with RS
178   encoder. Let i(x) denote information bits and g(x) denote generator polynomial. RS encoded bits can be
179   written as,

$$c(x) = i(x)g(x)$$

180   where c(x) represents RS encoded message bits. Now c(x) is transmitted via four transmitting antennas
181   using STBC coding. These signals are modulated and transmitted through a channel.

Figure. 3 depicts the STBC encoder and STBC decoder. STBC decoder comprises of Maximal Ratio
Combining (MRC) and Maximum Likelihood (ML) respectively. Since there are four receivers in the

system model, each receiver will receive either 0 or 1. The received signals can be represented as,

$$
\begin{bmatrix} r_1 \\ r_2 \\ r_3 \\ r_4 \\ r_5 \\ r_6 \\ r_7 \\ r_8 \end{bmatrix} = \begin{bmatrix} c_1 & c_2 & c_3 & c_4 \\ -c_2 & c_1 & -c_4 & c_3 \\ -c_3 & c_4 & c_1 & -c_2 \\ -c_4 & -c_3 & c_2 & c_1 \\ c_1^* & c_2^* & c_3^* & c_4^* \\ -c_2^* & c_1^* & -c_4^* & c_3^* \\ -c_3^* & c_4^* & c_1^* & -c_2^* \\ -c_4^* & -c_3^* & c_2^* & c_1^* \end{bmatrix} \times \begin{bmatrix} h_1 \\ h_2 \\ h_3 \\ h_4 \end{bmatrix} \times \begin{bmatrix} w_1 \\ w_2 \\ w_3 \\ w_4 \end{bmatrix}
$$

where w represents transmit beamforming weight vector i.e $w = [w1, w2, w3, w4]^T$ and $[h1, h2, h3, h4]^T$ is channel response.

In the above matrix, signals transmitted and received by four antennas are mentioned in Figure. 3. The output of the MRC in Figure 3 is explained in equation (4). Above matrics can be written as,

$$
\begin{bmatrix} r_1 \\ r_2 \\ r_3 \\ r_4 \\ r_5 \\ r_6 \\ r_7 \\ r_8 \end{bmatrix} = \begin{bmatrix} h_1 & h_2 & h_3 & h_4 \\ -h_2 & h_1 & -h_4 & h_3 \\ -h_3 & h_4 & h_1 & -h_2 \\ -h_4 & -h_3 & h_2 & h_1 \\ h_1^* & h_2^* & h_3^* & h_4^* \\ -h_2^* & h_1^* & -h_4^* & h_3^* \\ -h_3^* & h_4^* & h_1^* & -h_2^* \\ -h_4^* & -h_3^* & h_2^* & h_1^* \end{bmatrix} \times \begin{bmatrix} c_1 \\ c_2 \\ c_3 \\ c_4 \end{bmatrix} \times \begin{bmatrix} w_1 \\ w_2 \\ w_3 \\ w_4 \end{bmatrix}
$$

which can be represented as,

$$
\bar{r} = H_{\mathrm{ef}} c \bar{w} \tag{1}
$$

182   In equation (1) H_{ef} is effective channel response.
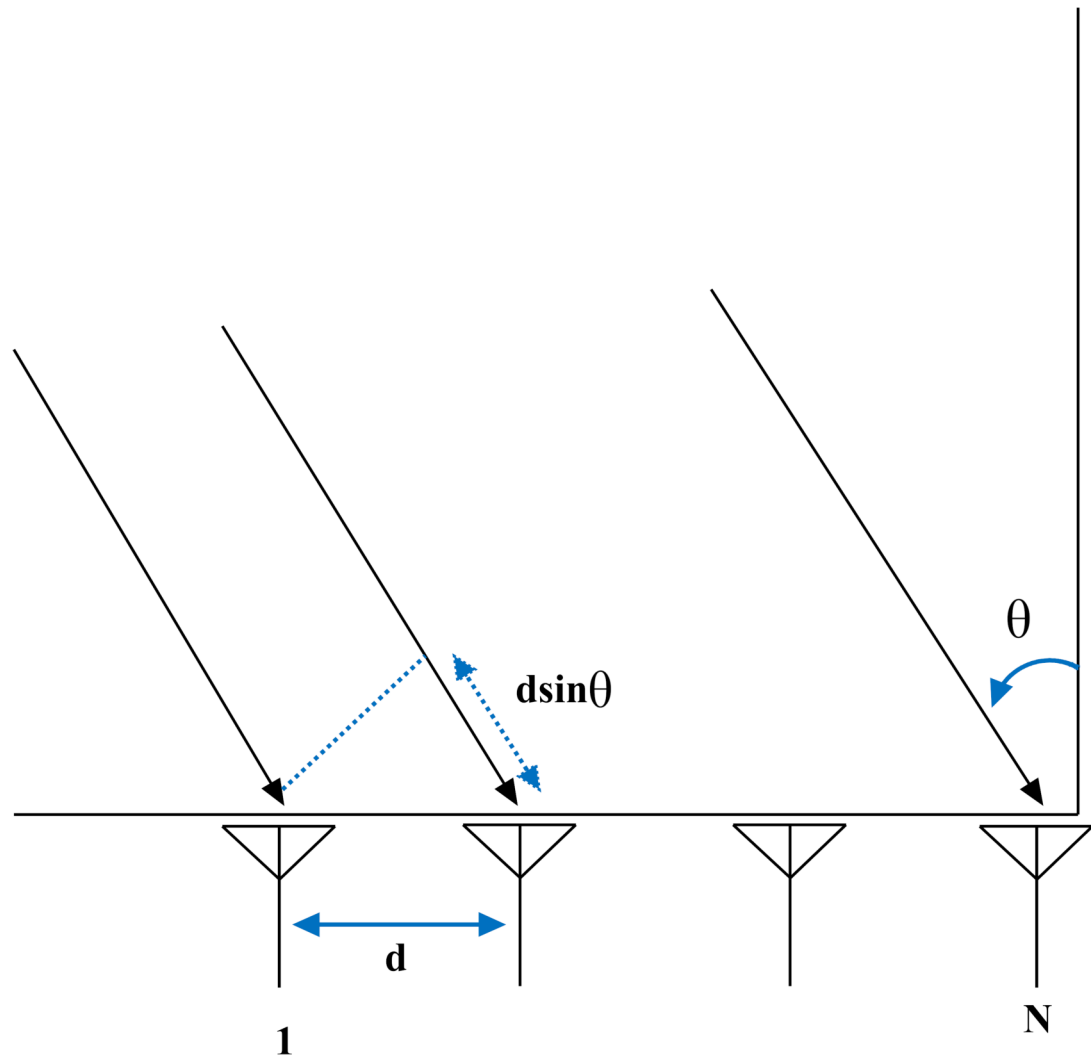
Figure 4. Beamforming in VANET

Corresponding weights w_i can be described below where w_i represents array factor and amplitude weight are applied by w_b (stepanets2019beamforming),

$$w_i = \sum_{b=1}^{N} w_b \exp^{jN\psi} \tag{2}$$

Equation (2) can be further simplified to normalized equation (3).

$$|w_i|^2 = \frac{1}{N} \left| \frac{sin(\frac{Nsin\psi}{2})}{sin\frac{\psi}{2}} \right| \tag{3}$$

where N represents the transmitting antennas, and ψ corresponds to the far-zone phase difference between adjacent elements, which can be calculated using the expression below (whitemillimeter).

$$\psi = sd sin\theta sin\phi + \Delta\psi$$

where θ represents angle of arrival described in Table 1 and ϕ represents angle of reflection. s corresponds to periodicity of complex weight which is $s = 2\pi/\lambda$ and d represents equidistant spacing between elements N as described in Figure. 4. $\Delta\psi$ can be computed using beam steering formula as follows.

$$\Delta\psi = \frac{2\theta}{\lambda}$$

183   The main lobe of an antenna array can be steered to a certain angle θ using phase offset $\Delta\psi$. ϕ is
184   computed using expression $\phi = \pi\sin\theta$.

Maximal Ratio Combining (MRC) at Receiver End

185

In MRC, multiple receivers are used for signal reception. Equation (4) describes the relation between the
signal arrived at MRC and transmitted by the MRC to ML (pericsoarua2012ber).

$$\widetilde{c} = H_{ef}^{H} r \tag{4}$$

186   In equation (4) $\widetilde{c}$ is output of MRC (four output signals), r represents input of MRC and $H_{ef}{}^{H}$ corresponds
187   to Hermitian matrix of effective channel response (pericsoarua2012ber).

Equation (4) can be written as,

$$
\begin{bmatrix} \widetilde{c_1} \\ \widetilde{c_2} \\ \widetilde{c_3} \\ \widetilde{c_4} \end{bmatrix} =
\begin{bmatrix}
h_1^* & h_2^* & h_3^* & h_4^* & h_1 & h_2 & h_3 & h_4 \\
h_2^* & -h_1^* & -h_4^* & h_3^* & h_2 & -h_1 & -h_4 & h_3 \\
h_3^* & h_4^* & -h_1^* & -h_2^* & h_3 & h_4 & -h_1 & -h_2 \\
-h_4^* & -h_3^* & h_2^* & -h_1^* & -h_4 & -h_3 & h_2 & -h_1
\end{bmatrix} \times
\begin{bmatrix} r_1 \\ r_2 \\ r_3 \\ r_4 \\ r_1^* \\ r_2^* \\ r_3^* \\ r_4^* \end{bmatrix}
$$

188   The probability of error in MRC Rayleigh fading is described in equation (5) (goldsmith2005wireless)[eq
189   (7.18)].

$$p_e = \left(\frac{1-\Gamma}{2}\right)^L \sum_{l=0}^{L-1} \binom{L-1+l}{l} \left(\frac{1+\Gamma}{2}\right)^l \tag{5}$$

where L represents the number of the receiver. In equation (5), Γ can be written as,

$$\Gamma = \sqrt{\frac{\gamma}{1+\gamma}} \tag{6}$$

Maximum Likelihood (ML) Estimator

190

191   After MRC, signals c(x) are sent to ML estimator as mentioned in equation (7). Afterward RS decoder
192   receives signals and processes them.

$$y(x) = c(x) + e(x) \tag{7}$$

The signal-to-noise ratio per receive antenna can be written as,

$$\gamma_1 = \frac{w_i.m.P_t.N.R_c}{\sigma^2} \tag{8}$$

193   Where P_t represents transmitted power in dB, m represents modulation index, σ corresponds to standard
194   deviation and R_c denotes code rate. SNR per symbol can be computed as,

$$\gamma^{STBC} = \frac{\bar{\gamma}}{NR_c}(\| H \|)_F^2 \tag{9}$$

195   Where $\| H \|^2{}_F$ represents Frobenius norm of matrix H.

196 **RS Error Probability in Rayleigh Channel (Non Line of Sight Model)**

197 In this subsection, RS channel probability in Rayleigh fading is determined, i.e, Non Line of Sight (NLOS)
198 model. RS can detect and correct t= n-k/2 symbol errors where n represents the number of coded bits and
199 k corresponds to the number of information bits. For detection and correction of errors d_{min} should be
200 more than n-k+1.

Probability of symbol error P_s is given as,

$$P_s = \sum_{t+1}^{n} \binom{n}{j} p_e^j (1 - p_e)^{n-j} \tag{10}$$

where p_e is calculated using equation (4) and j=t+1. The probability of error of RS in Rayleigh fading is
written as,

$$P_e = \int_0^{+\infty} P_s \frac{1}{\gamma} exp^{-\frac{p_e}{\gamma}} dp_e \tag{11}$$

Substituting Eq. (10) into Eq. (11) gives,

$$P_e = \int_0^{+\infty} \sum_{t+1}^{n} \binom{n}{j} p_e^j (1 - p_e)^{n-j} dp_e \cdot \frac{1}{\gamma} exp^{-\frac{p_e}{\gamma}} \tag{12}$$

Using(gradshteyn1963table)[eq.(1.111),p.25]

$$(a+x)^n = \sum_{t=0}^{n} \binom{n}{j} a^j x^{n-j} \tag{13}$$

Expression (12) can be modified to,

$$P_e = \int_0^{+\infty} (p_e + x)^n \frac{1}{\gamma} exp^{-\frac{p_e}{\gamma}} dp_e \tag{14}$$

Applying integration,

$$P_e = \frac{1}{\gamma} exp^{-\frac{p_e}{\gamma}} \int_0^{+\infty} (p_e + x)^n \ dp_e -$$
$$\int_0^{+\infty} (\frac{1}{\gamma} exp^{-\frac{p_e}{\gamma}} \frac{d}{dp_e}) \int_0^{+\infty} (p_e + x)^n dp_e \tag{15}$$

$$P_e = \frac{1}{\gamma} exp^{-\frac{p_e}{\gamma}} \cdot \frac{(p_e + x)^{n+1}}{n+1} -$$
$$\int_0^{+\infty} (\frac{1}{\gamma} exp^{-\frac{p_e}{\gamma}} \frac{d}{dp_e}) \frac{(p_e + x)^{n+1}}{n+1} \ dp_e \tag{16}$$

201 Applying limits to p_e.

$$P_e = -\frac{1}{\gamma} exp^{-\frac{p_e}{\gamma}} \frac{(x)^{n+1}}{n+1} - \int_0^{+\infty} \frac{1}{\gamma} exp^{-\frac{p_e}{\gamma}} \frac{d}{dp_e})$$
$$(-\frac{(x)^{n+1}}{n+1}) dp_e \tag{17}$$

Applying differentiation,

$$P_e = -\frac{1}{\gamma} exp^{-\frac{p_e}{\gamma}} \frac{(x)^{n+1}}{n+1} + \int_0^{+\infty} \frac{1}{\gamma} exp^{-\frac{p_e}{\gamma}}$$
$$(-\frac{1}{\gamma}) \frac{(x)^{n+1}}{n+1} dp_e \tag{18}$$

Applying integration finally we have,

$$P_e = -\frac{1}{\gamma} exp^{-\frac{p_e}{\gamma}} \frac{(x)^{n+1}}{n+1} - \frac{1}{\gamma^2} \frac{1}{\frac{1}{\gamma}} \frac{(x)^{n+1}}{n+1} \tag{19}$$

202 The equation (19) represents closed-form approximation of BER of RS in Rayleigh fading.

RS Error Probability in AWGN Channel (Line of Sight Model)

BER of AWGN Channel can be written as (goldsmith2005wireless)[eq (6.3)],

$$BER = \frac{p_e}{log_2 M} \tag{20}$$

The BER of RS in AWGN channel can be written as,

$$P_e = \int_0^{+\infty} \frac{p_e}{log_2 M} \sum_{t+1}^{n} \binom{n}{j} . p_e^j (1 - p_e)^{n-j} \, dp_e \tag{21}$$

Using expression (14), we have,

$$P_e = \int_0^{+\infty} (p_e + x)^n \frac{p_e}{log_2 M} \, dp_e \tag{22}$$

After manipulating above expression,

$$P_e = \frac{p_e}{log_2 M} \frac{(p_e + x)^{n+1}}{n+1} - \int_0^{+\infty} \left(\frac{1}{log_2 M} \frac{(p_e + x)^{n+1}}{n+1} \right) \, dp_e \tag{23}$$

After solving above expression,

$$P_e = -\frac{p_e}{log_2 M} \frac{x^{n+1}}{n+1} + \int_0^{+\infty} \frac{1}{log_2 M} \frac{x^{n+1}}{n+1} \, dp_e \tag{24}$$

After integration, second term becomes 0.

$$P_e = \frac{p_e}{log_2 M} \frac{x^{n+1}}{n+1} \tag{25}$$

Equation (25) represents closed-form approximation of bit error probability of RS in AWGN channel.

Doppler Effect in Proposed Model

Consider the proposed model in Figure 1 in which the vehicles are traveling with velocity v which is varying from 25 km/h to 250 km/h. The closed-form expression of RS BER probability in Rayleigh fading i.e equation (19) is mentioned below,

$$P_e = -\frac{1}{\overline{\gamma}} exp^{-\frac{p_e}{\overline{\gamma}}} \frac{(x)^{n+1}}{n+1} - \frac{1}{\overline{\gamma}^2} \frac{1}{\frac{1}{\overline{\gamma}}} \frac{(x)^{n+1}}{n+1} \tag{26}$$

SNR under Doppler effect can be written as,

$$\overline{\gamma} = \frac{A^2}{2 * \sigma^2} . f_d$$

where A corresponds to magnitude of signal and f_d represents Doppler shift. Plugging value of $\overline{\gamma}$ in expression (26),

$$P_e = \frac{2.\sigma^2}{f_d} . exp^{\frac{p_e.2.\sigma}{f_d}} . \frac{x^{n+1}}{n+1} + \frac{2.\sigma^2}{f_d} . \frac{x^{n+1}}{n+1}$$

Probability density function of f_d can be written as,

$$P_{ed} = \int_0^{+\infty} \frac{1}{\gamma} . exp^{-\frac{f_d}{\gamma}} . P_e df_d \tag{27}$$

Substituting P_e in above expression,

$$P_{ed} = \int_0^{+\infty} \left(\frac{1}{\gamma} . exp^{-\frac{f_d}{\gamma}} \right) . \left(\frac{2.\sigma^2}{f_d} . exp^{\frac{p_e.2.\sigma}{f_d}} . \frac{x^{n+1}}{n+1} + \frac{2.\sigma^2}{f_d} . \frac{x^{n+1}}{n+1} \right) df_d \tag{28}$$

$$P_{ed} = \int_0^{+\infty} \frac{1}{\gamma}.exp^{-\frac{f_d}{\gamma} - \frac{pe.2.\sigma^2}{f_d}} . \frac{x^{n+1}}{n+1} . \frac{2.\sigma^2}{f_d} +$$
$$\frac{1}{\gamma}.exp^{-\frac{f_d}{\gamma}} . \frac{2.\sigma^2}{f_d} . \frac{x^{n+1}}{n+1} df_d \tag{29}$$

206   Manipulating above expression,

$$P_{ed} = \frac{1}{\gamma} . \frac{x^{n+1}}{n+1} \int_0^{+\infty} exp^{-\frac{f_d}{\gamma} - \frac{pe.2.\sigma^2}{f_d}} \frac{2.\sigma^2}{f_d} +$$
$$\int_0^{+\infty} exp^{-\frac{f_d}{\gamma}} . \frac{2.\sigma^2}{f_d} \tag{30}$$

Applying integration by parts,

$$P_{ed} = \frac{1}{\gamma} . \frac{x^{n+1}}{n+1} . (\frac{2.\sigma^2}{f_d} . \int_0^{+\infty} exp^{-\frac{f_d}{\gamma} - \frac{pe.2.\sigma^2}{f_d}} -$$
$$\int_0^{+\infty} (\frac{2.\sigma^2}{f_d} \frac{d}{df}) \int_0^{+\infty} exp^{-\frac{f_d}{\gamma} - \frac{pe.2.\sigma^2}{f_d}} +$$
$$exp^{-\frac{f_d}{\gamma}} \int_0^{+\infty} \frac{2.\sigma^2}{f_d} - \int_0^{+\infty} exp^{-\frac{f_d}{\gamma}} \frac{d}{df} . \int_0^{+\infty} \frac{2.\sigma^2}{f_d}) df_d \tag{31}$$

In (gradshteyn1963table)[eq.(3.325),p.336],

$$\int_0^{+\infty} exp^{-\frac{f_d}{\gamma} - \frac{pe.2.\sigma^2}{f_d}} = \frac{1}{2} . \sqrt{\frac{pi}{\frac{1}{\gamma}}} . exp^{-2.\sqrt{\frac{2.\sigma^2.pe}{\gamma}}}$$

Replacing above expression in expression (31) yields,

$$P_{ed} = \frac{1}{\gamma} . \frac{x^{n+1}}{n+1} . (\frac{2.\sigma^2}{f_d} . \frac{1}{2} . \sqrt{\frac{pi}{\frac{1}{\gamma}}} . exp^{-2.\sqrt{\frac{2.\sigma^2.pe}{\gamma}}} + \int_0^{+\infty}$$
$$(\frac{2.\sigma^2}{f_d^2}) . \frac{1}{2} . \sqrt{\frac{pi}{\frac{1}{\gamma}}} . exp^{-2.\sqrt{\frac{2.\sigma^2.pe}{\gamma}}} + \tag{32}$$
$$exp^{-\frac{f_d}{\gamma}} \int_0^{+\infty} \frac{2.\sigma^2}{f_d} - \int_0^{+\infty} exp^{-\frac{f_d}{\gamma}} \frac{d}{df} . \int_0^{+\infty} \frac{2.\sigma^2}{f_d})$$

Applying integration and limits,

$$P_{ed} = \frac{1}{\gamma} . \frac{x^{n+1}}{n+1} . (\frac{2.\sigma^2}{f_d} . \frac{1}{2} . \sqrt{\frac{pi}{\frac{1}{\gamma}}} . exp^{-2.\sqrt{\frac{2.\sigma^2.pe}{\gamma}}}$$
$$-exp^{\frac{f_d}{\gamma}} . 2.\sigma^2 + 2.\sigma^2 . \frac{1}{\gamma} . \int_0^{+\infty} exp^{-\frac{f_d}{\gamma}}) \tag{33}$$

Manipulating above expression yields to,

$$P_{ed} = \frac{1}{\gamma} . \frac{x^{n+1}}{n+1} . (\frac{2.\sigma^2}{f_d} . \frac{1}{2} . \sqrt{\frac{pi}{\frac{1}{\gamma}}} . exp^{-2.\sqrt{\frac{2.\sigma^2.pe}{\gamma}}}$$
$$-exp^{-\frac{f_d}{\gamma}} . 2.\sigma^2 + \frac{1}{\gamma} . \frac{1}{\frac{1}{\gamma}} . 2.\sigma^2) \tag{34}$$

207   Applying integration and limits,

$$P_{ed} = \frac{1}{\gamma} \cdot \frac{x^{n+1}}{n+1} \cdot (\frac{2.\sigma^2}{f_d} \cdot \frac{1}{2} \cdot \sqrt{\frac{pi}{\frac{1}{\gamma}}} . exp^{-2.\sqrt{\frac{2.\sigma^2.pe}{\gamma}}} - exp^{-\frac{f_d}{\gamma}} .$$

$$2.\sigma^2 + 2 * \sigma^2)$$

(35)

Equation (35) represents RS coded Doppler shift expression in Rayleigh fading.

RESULTS AND DISCUSSION

This section comprises of results and discussion of the proposed model. Matlab is used as a simulation platform.

In this research, LOS, NLOS, number of antenna elements N, equidistant spacing d (30 mm, 40 mm, 50 mm) and relative velocity v (25 km/h, 100 km/h, 250 km/h) are used as use cases.

Figure. 5 and Figure. 6 show the impact of the number of transmitting antennas and their equidistant spacing on directivity.

The simulation parameters are shown in Table 1.

Table 1. Beamforming Simulation Parameters

Parameter	Value
Frequency	60GHz
θ	-15° to 15°
N	2,3,4
d	30 mm, 40 mm, 50 mm

From Figure. 5 it can be remarked that by increasing the number of transmitting antennas i.e. N which is varying from 2 to 4, directivity increases. When directivity increases, the beam gain increases and thus, the probability of signal loss reduces. d=50 mm is used in simulation. However, the effect of increasing the number of transmitting antennas results in a larger number of side lobes as shown in Figure. 5. In beamforming, linear arrays with increasing equidistant element spacing will also produce grating lobes as described in Figure. 6. These grating lobes are unwanted energy that will be radiated to or received from undesired directions. If the equidistant spacing exceeds half a wavelength grating lobes start to appear in the visible region. To avoid this phenomenon following condition must be kept as,

$$d < \frac{\lambda}{2}$$

In case the distance between transmitting antennas exceeds one wavelength, the grating lobe levels start to equal the main lobe level. Since the array factor is periodic in nature, grating lobes will start to appear in the visible region coming from the invisible region. In this case, scan angle will be restricted. So the maximum value of scan angle must be,

$$sin|\theta| = \frac{\lambda}{d} - 1$$
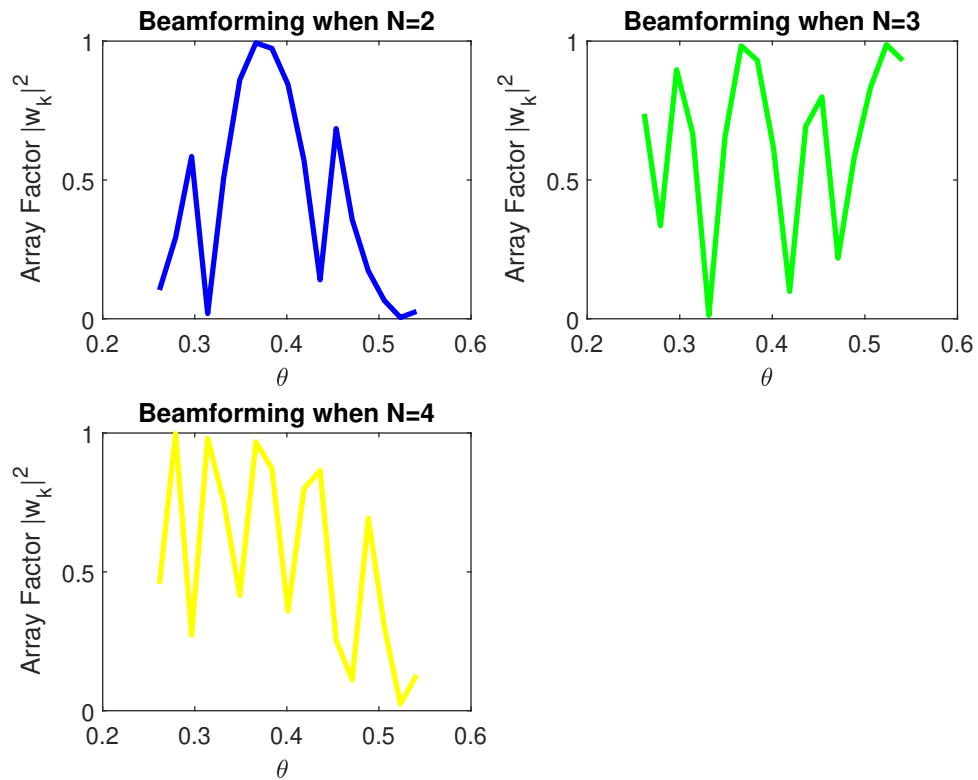
Figure 5. Signal received after Beamforming when number of elements are increasing
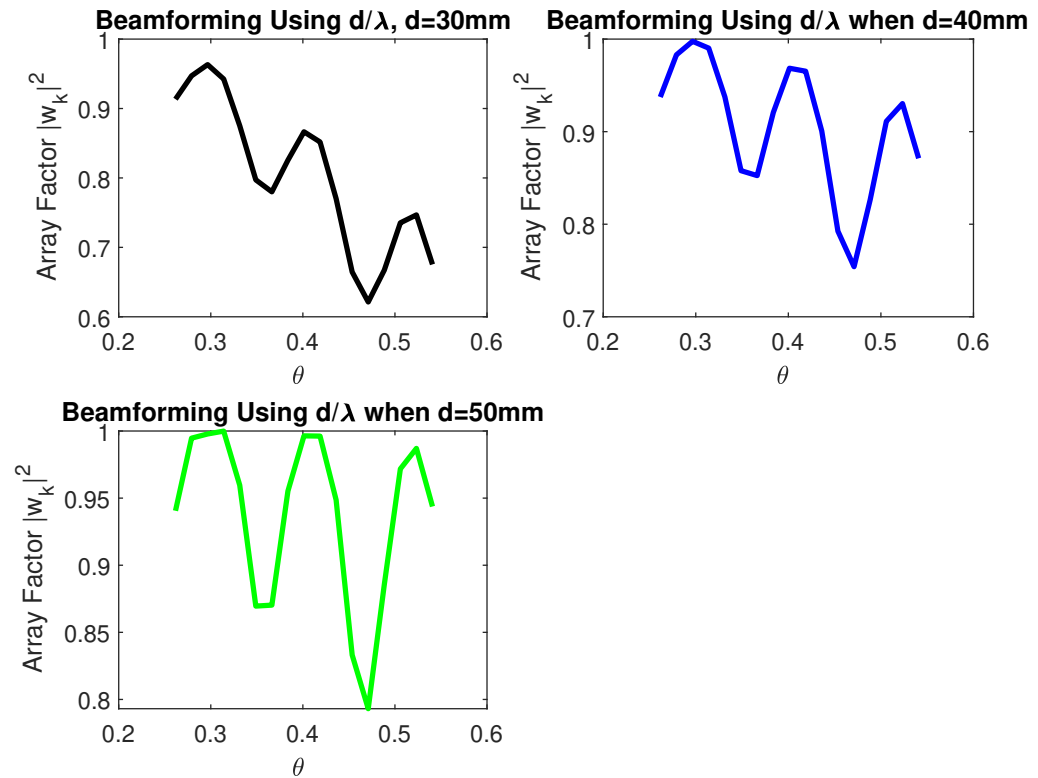
Figure 6. Signal received after Beamforming when distance between elements is increasing
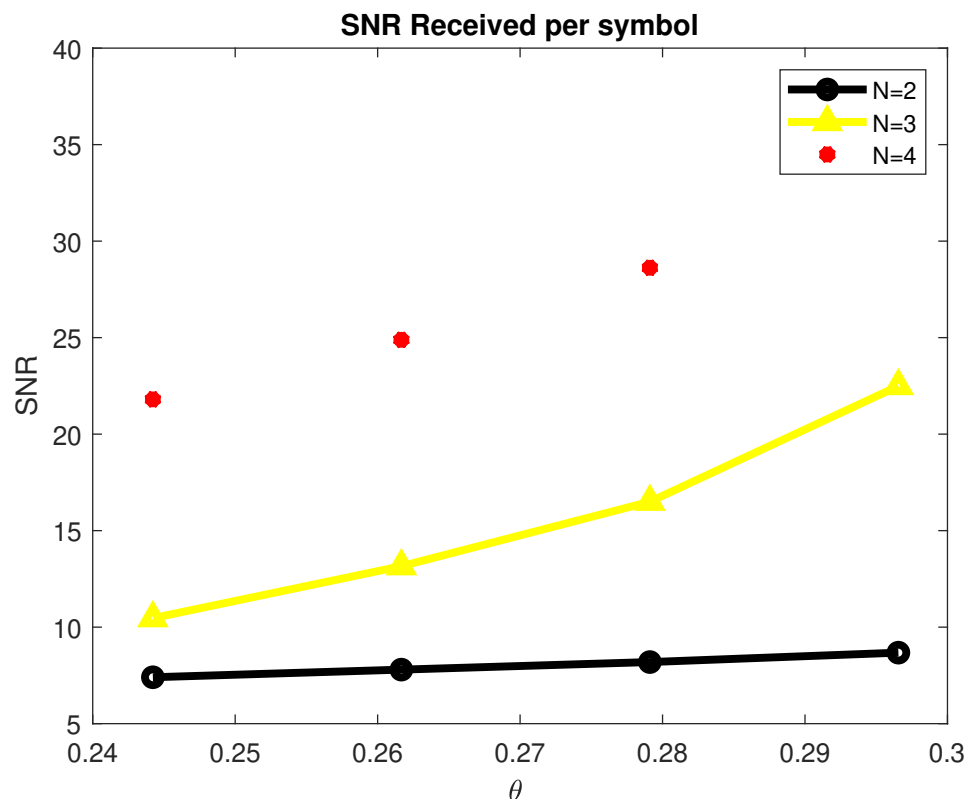
Figure 7. SNR per symbol in Maximal Likelihood Detector

Table 2. Simulation Parameters

Parameter	Value
No. of transmitting elements N	4
Transmit power P_t	10dB
modulation index m	1
standard deviation σ^2	9
Code Rate R_c	.9
Carrier frequency f $_c$	60 GHz
Data rate	7.31 Mbps
Packet size	100 Bytes

225   For SNR calculation equation (8) is used. Simulation parameters are describe in Table 2. SNR per
226 symbol is computed in a ML detector using expression (9). Figure. 7 displays the graph of SNR per
227 symbol versus angle of reflection theta. When increasing the angle of reflection, SNR per symbol also
228 rises. By increasing the number of transmitters to N=4, SNR also gets high. The capacity of a system is
229 directly proportional to the number of transmitters. The capacity of our system is 2.5 bits/s/Hz when there
230 are four transmitters as shown in Figure. 8.
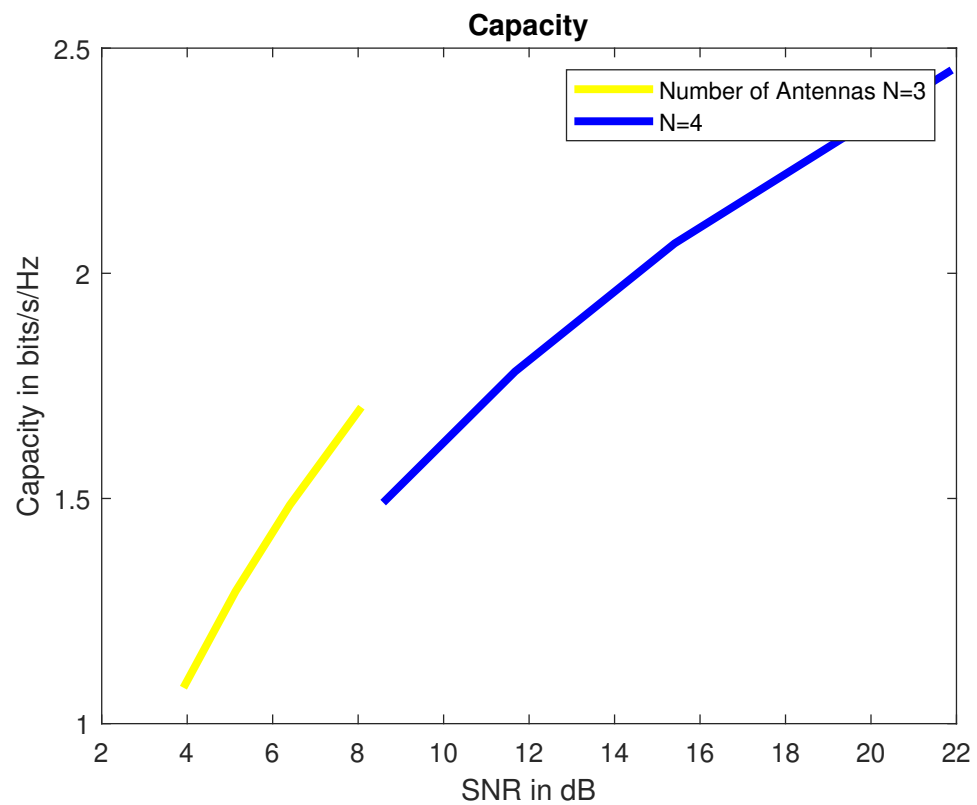
Figure 8. Capacity in bits/s/Hz
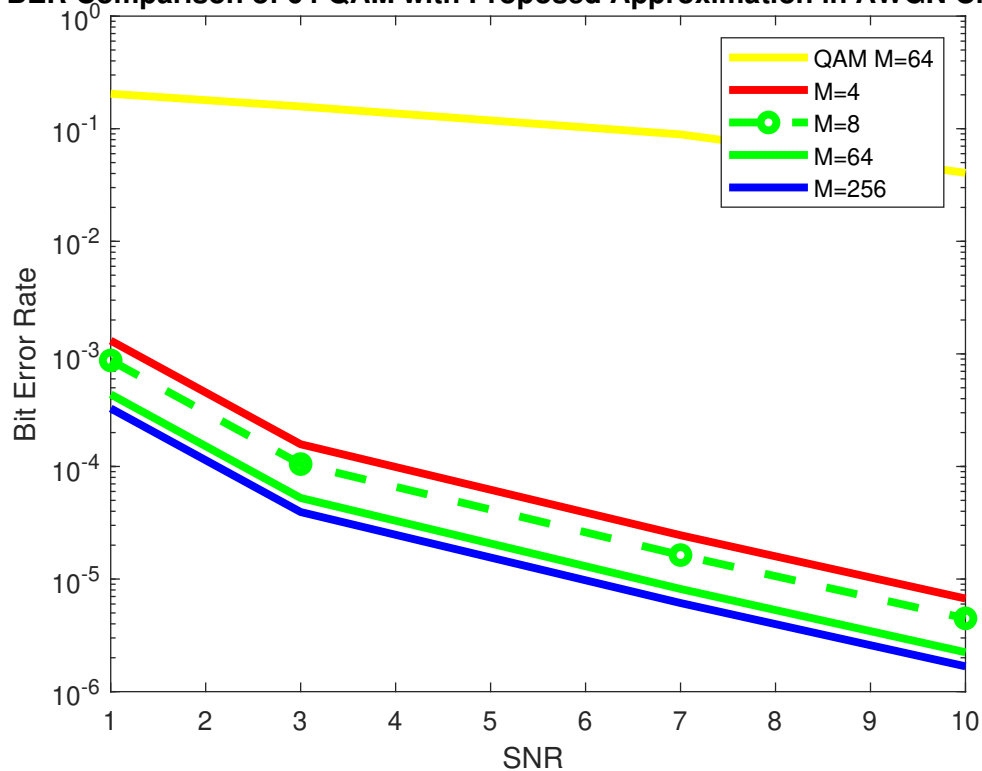
Figure 9. RS BER Comparison of 64QAM with Proposed Approximation
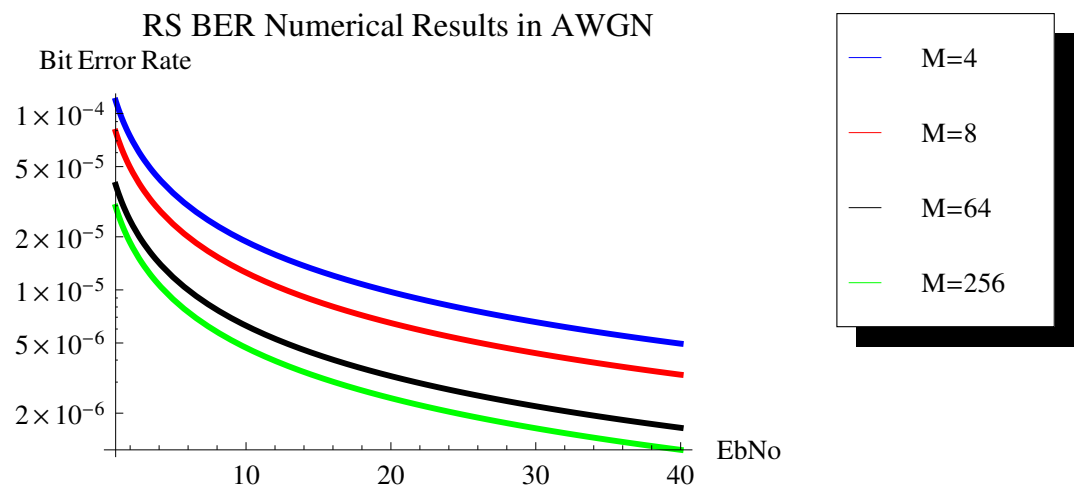
Figure 10. RS BER Comparison of 64QAM with Proposed Approximation

Figure 11. RS BER Comparison of 4PSK with Proposed Approximation
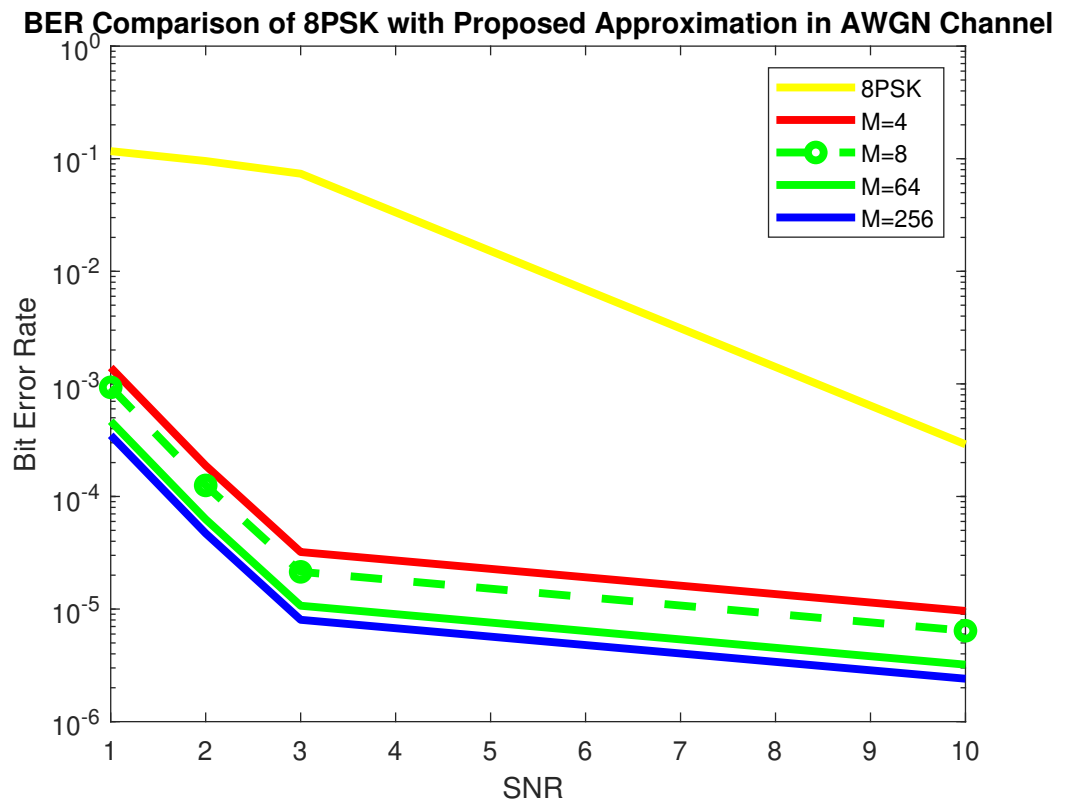
Figure 12. RS BER Comparison of 8PSK with Proposed Approximation
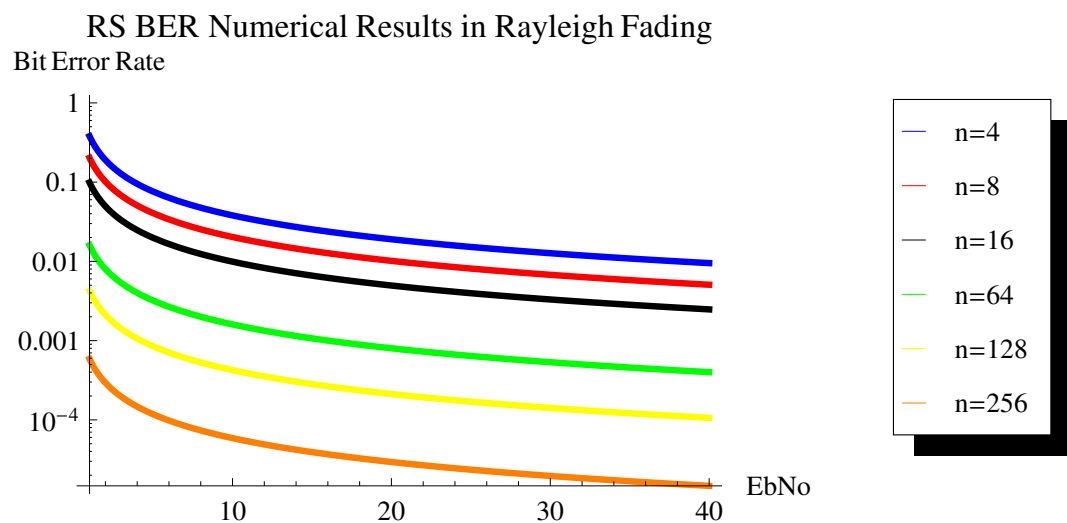
Figure 13. RS BER Proposed Approximation Numerical Results in Rayleigh Channel
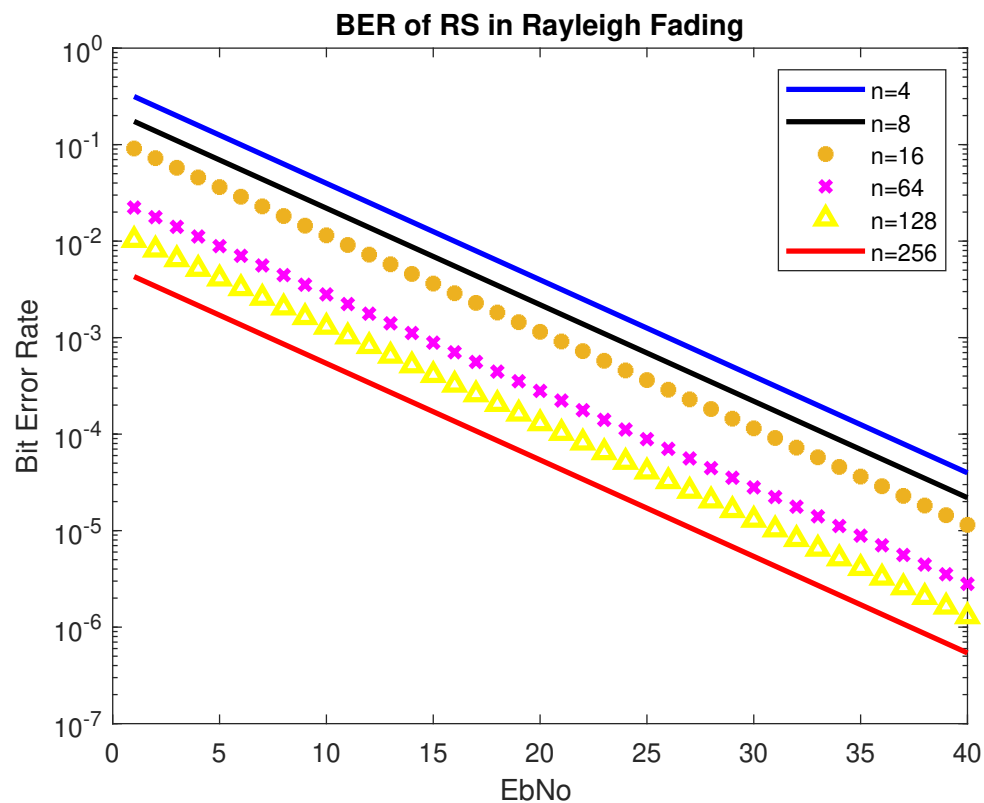
Figure 14. BER of RS in Rayleigh Fading
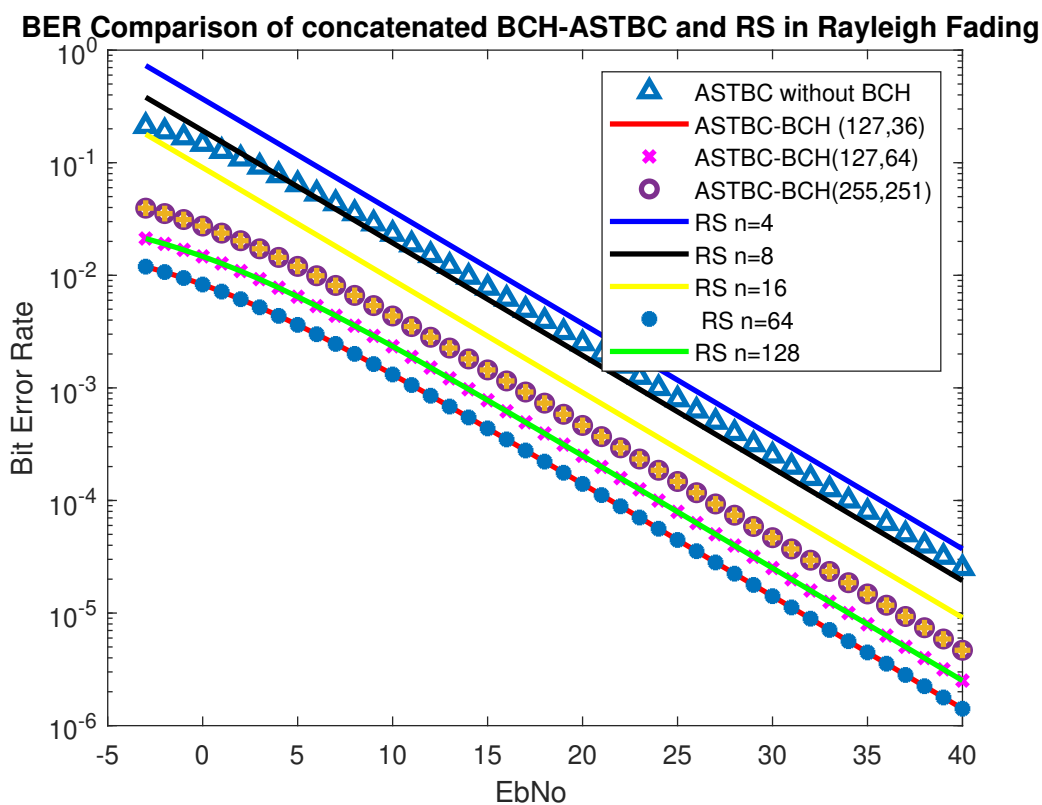
Figure 15. Comparison of BER of STBC-RS with BCH-ASTBC
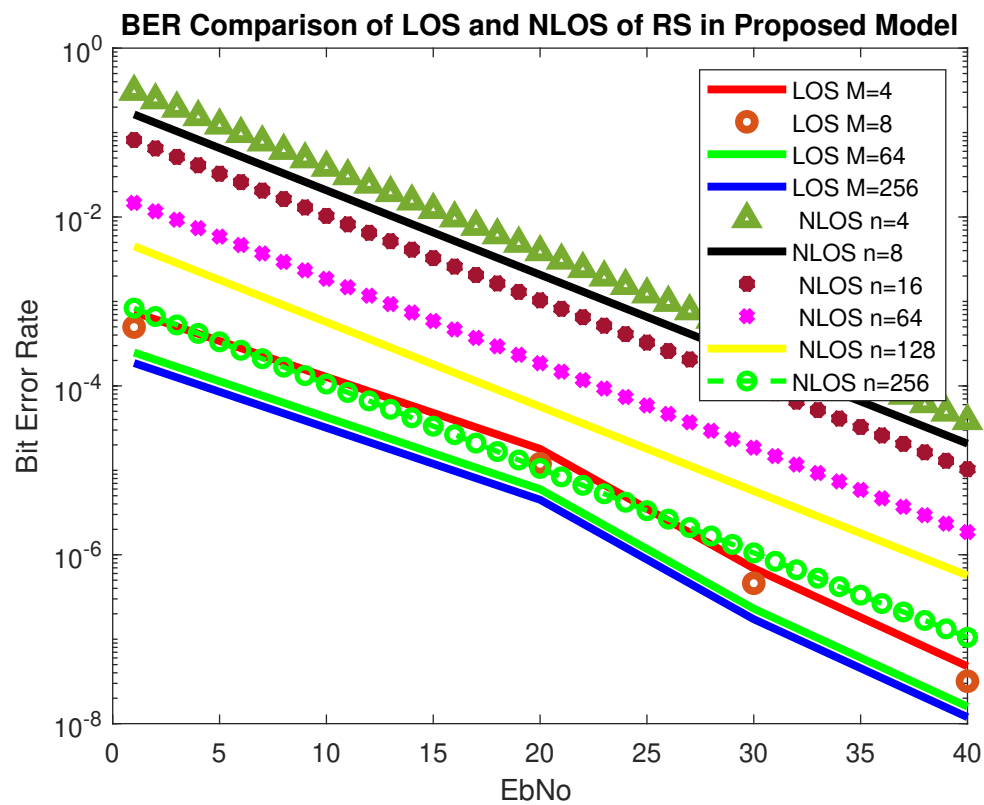
Figure 16. BER Comparison of RS in Rayleigh Fading and AWGN Channel
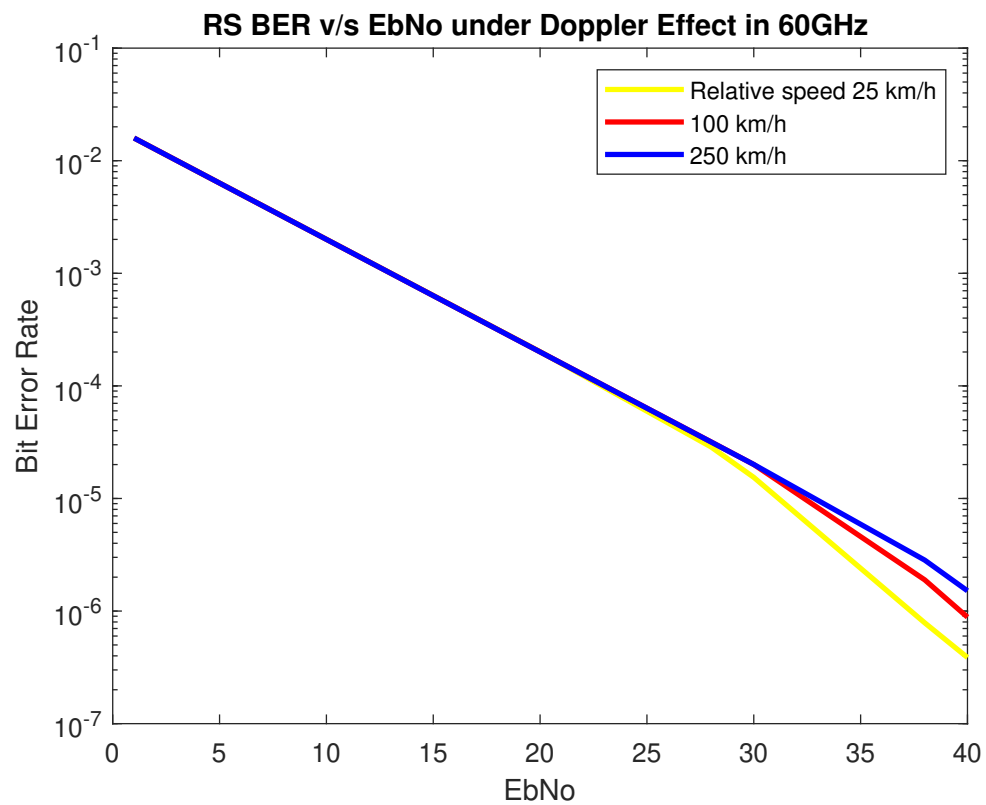
Figure 17. BER of RS Under Doppler Effect
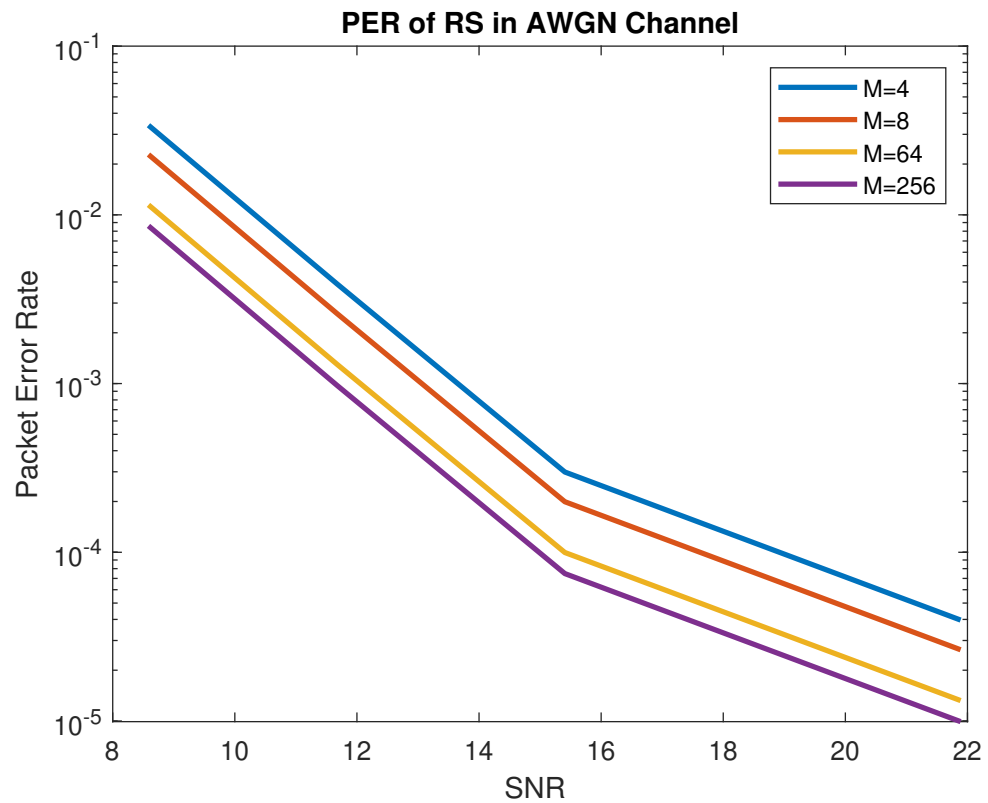
Figure 18. PER (Packet size = 100 Bytes) of RS in AWGN Channel
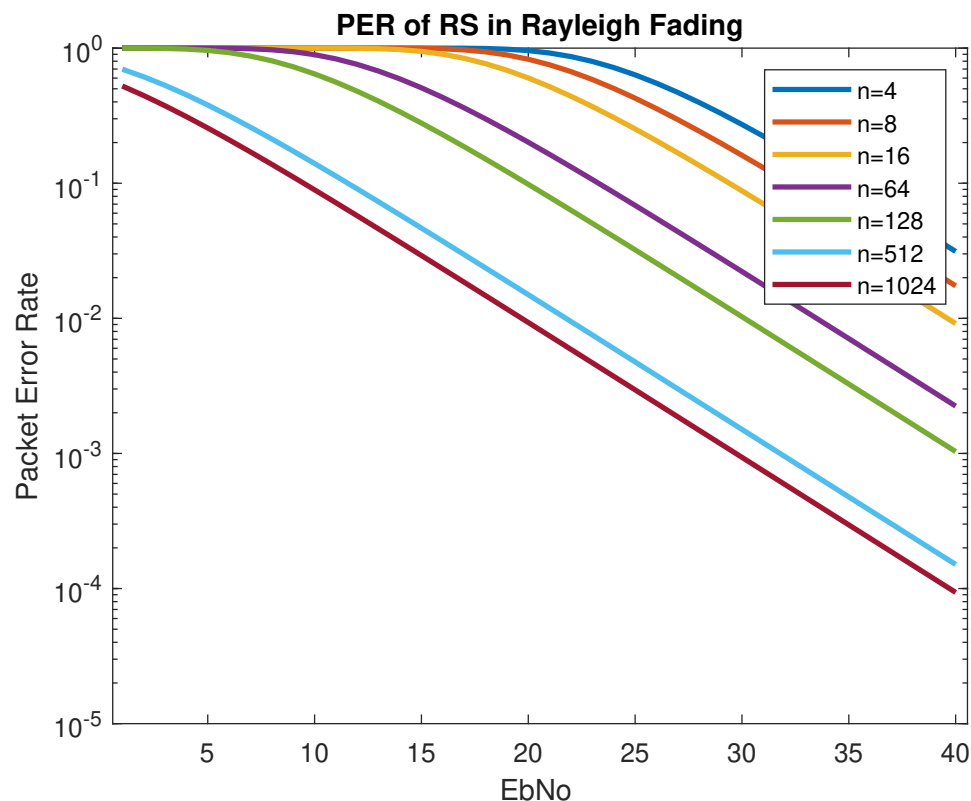
Figure 19. PER (Packet size = 100 Bytes) of RS in Rayleigh Fading

Figure. 9 shows the simulation results and Figure. 10 depicts the numerical results of closed-form approximation of RS BER in the AWGN channel. It can be remarked from both figures that the results verify each other. On comparing our result with the traditional 64-QAM system it can figure out that the BER of 64-QAM is higher than our proposed approximation. The BER of the M-PSK is compared with our expression described in Figure. 11 and Figure. 12. The BER of M-PSK system is getting low on account of decreasing modulation order M. The BER of the 4PSK system is lower than the 8PSK system. However, the BER of proposed approximation gets low on account of increasing modulation order M. So our result outperforms both the 64-QAM and M-PSK system. The simulation parameter described in Table 2.

Figure. 13 and Figure. 14 show the numerical results and simulation results of closed-form approximation of RS error probability in the Rayleigh channel. On comparing results based on n, it can be observed that error probability is getting depleted by increasing n.

Table 3. Comparative Analysis of proposed model with previous studies in terms of BER

Sr. No.	Paper	Approach	BER (Propagation Channel NLOS/LOS)	BER (Modulation and Coding)	Comparison With Proposed Technique using Modulation and Coding	Comparison With Proposed Technique using LOS/NLOS
1	(al2017enhancing)	RS performance is increased using multi-path propagation in LOS and NLOS scenario	10^{-5}	x	x	10^{-5}, 10^{-6}
2	(mergu2016performance)	RS performance is analyzed using RS codes concatenated with Convolutional Codes over AWGN Channel	10^{-2}	Convolutional Codes, 10^{-2}	10^{-5}	10^{-5}
3	(Tiwari2013BERPO)	Comparison Analysis of LDPC and RS codes on multiple antennas using AWGN channel	10^{-2} to 10^{-3}	BPSK, QPSK, LDPC, RS, 10^{-2} to 10^{-3}	10^{-5}	10^{-5}
4	(indoonundon2021overview)	To achieve ultra reliable low latency communication in 5G, a detailed analysis of coding schemes was conducted	x	BER lies between 10^{-6} to 10^{-7}	10^{-7}	x
5	(saleh2019improving)	Communication reliability was improved using different diversity schemes	x	BPSK, MRC outperforms other techniques	10^{-5}	x
6	(hajiyat2019channel)	The reliability of VANET was evaluated using turbo, Low Density Parity Check Code (LDPC), Polar code, Systematic Convolutional Codes (SCC), and Non-Systematic Convolutional Codes (NSCC) coding types	x	10^{-7}	10^{-6}	x
7	(hamarsheh2022robust)	MIMO-FFH-OFDM	x	10^{-4}	10^{-5}	x
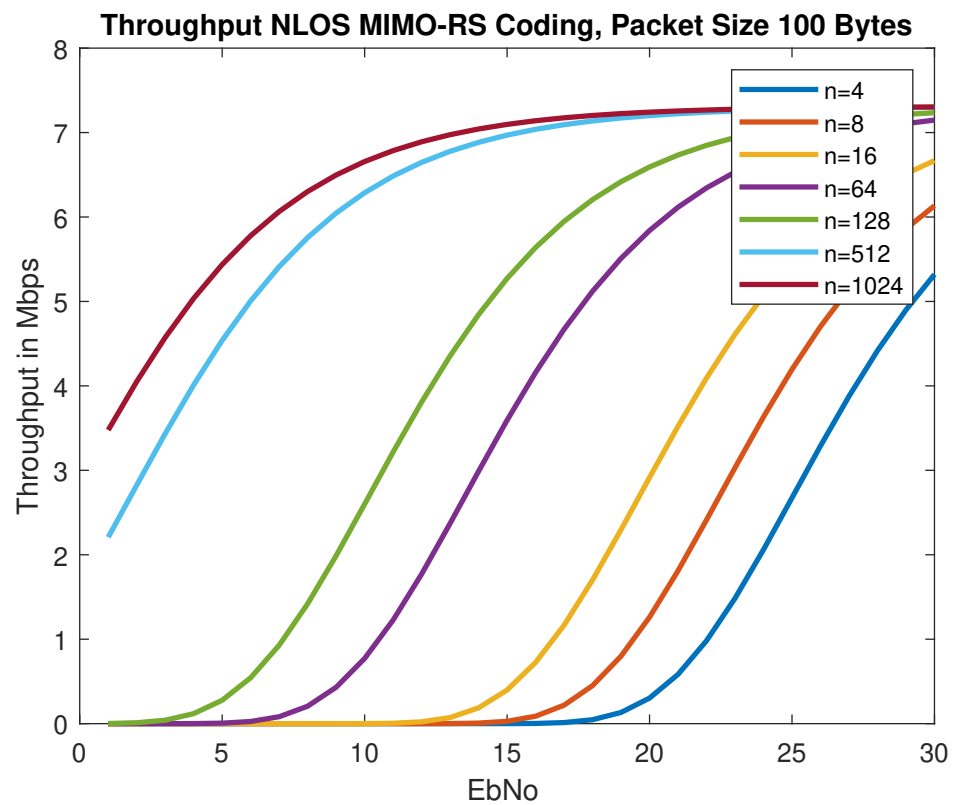
Figure 20. Throughput of MIMO-RS (Packet size = 100 Bytes) in NLOS
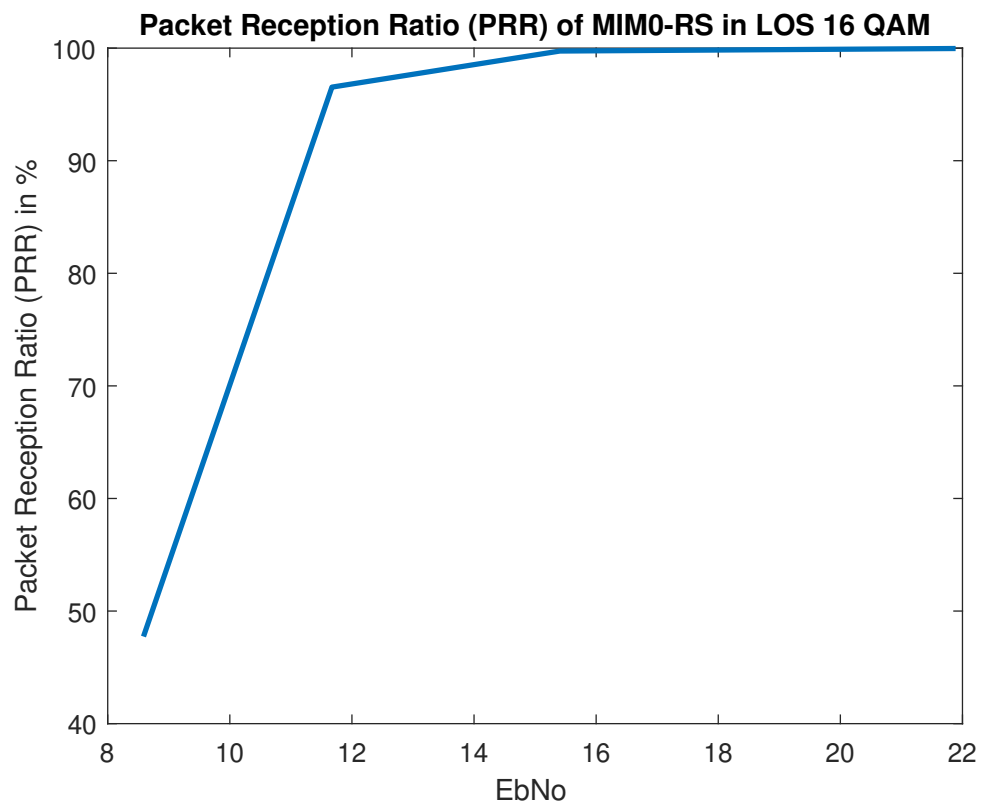
Figure 21. Packet Reception Ratio (PRR) of MIMO-RS in LOS (Packet size = 100 Bytes)

Table 4. PER Analysis of Proposed Approach (Modulation) with IEEE 802.11p and NR V2X

Comparison Analysis of Proposed Approach with IEEE 802.11bd and V2X (anwar2019physical)		
VANET Communication Standards	Modulation	PER
IEEE 802.11bd	QPSK/64 QAM	10^{-3}
NR V2X	QPSK/64 QAM	10^{-3} / 10^{-2}
Proposed Methodology	BPSK/16/QAM/64QAM	10^{-4}/10^{-5}
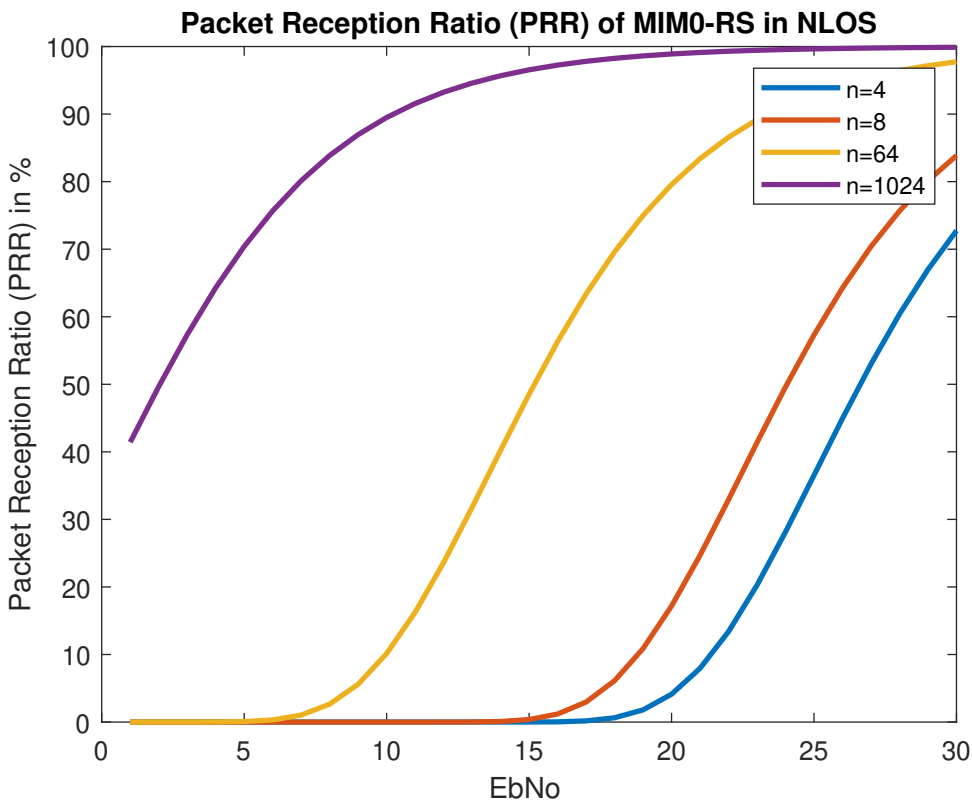
Figure 22. Packet Reception Ratio (PRR) of MIMO-RS in NLOS (Packet size = 100 Bytes)

Table 3 illustrates the comparative analysis of proposed model with previous studies in terms of BER. The results are analyzed using NLOS/LOS cases and modulation and coding types from different studies.

The performance of the proposed system is compared with (electronics10090992) in which concatenated BCH-ASTBC was used for VANET commmunication. Results are described in Figure. 15. The performance of BCH-ASTBC with code rate (127,36) is similar to RS BER at n=64. The similar curve was also obtained for BCH-ASTBC with code rate (127,64) and RS BER at n=128. The BER curve of ASTBC without BCH code is in between RS BER at n=4 and RS BER at n=8. Figure. 16 depicts the comparative analysis of AWGN channel and Rayleigh channel. Figure. 17 displays result of Doppler shift in RS coding. The change in frequency causes frequency offset is the main source of high BER in VANET communications.

Comparison Analysis of proposed approach with IEEE 802.11bd and 3GPP V2X Communication

Table 5. PER Analysis of Proposed Approach (Coding) with IEEE 802.11p and NR V2X

Comparison Analysis of Proposed Approach with IEEE 802.11bd and V2X (anwar2020performance)			
VANET Communication Standards	Modulation	Coding	PER
IEEE 802.11bd	BPSK	Convolutional, LDPC, Turbo, Polar	10^{-3}
NR V2X	BPSK	Convolutional, LDPC, Turbo, Polar	10^{-3}
Proposed Methodology	BPSK	RS	10^{-4}, 10^{-5}

Table 6. Throughput Analysis of Proposed Approach with IEEE 802.11p and NR V2X

Throughput Analysis of Proposed Approach with IEEE 802.11bd and V2X (anwar2020performance) (triwinarko2021phy)		
VANET Communication Standards	Coding	Throughput
IEEE 802.11bd	LDPC	7 Mbps
V2X	Convolutional, LDPC, Turbo, Polar	4 Mbps
Proposed Methodology	RS	7 Mbps

In this subsection, the performance of the proposed system is compared with IEEE 802.11bd and 5G NR V2X standard. The PER of LOS model is described in Figure. 18. The PER of NLOS model (Rayleigh fading) is shown in Figure. 19.

The performance of upcoming technologies i.e 5G NRV2X and IEEE 802.11bd V2V communications was analyzed in (anwar2019physical). Comparing RS Packet Error Rate (PER) in AWGN channel shown in Figure. 18 with 802.11 bd and NR V2X 64-QAM in (anwar2019physical) it can be observed that the performance of our proposed RS model is optimal. Results are displayed in Table 4.

According to (anwar2020performance) the performance of LDPC is marginal in V2X communication. The performance of proposed model outperforms LDPC, Turbo, Polar and Convolutional coding. Because the reliability of the system gets better since low PER is received in Figure. 19. Table 5 displays the comparison between proposed method with IEEE 802.11bd and V2X using PER. Comparing RS performance under Doppler Effect shown in Figure. 17, it can be remarked that RS performance is optimal.

In (triwinarko2021phy) the performance of various modulations schemes was evaluated on IEEE 802.11bd using LDPC. The packet size of 100 bytes was used for simulation. It can be observed that the RS error control coding gives us high reliability, as mentioned in Figure. 18 and Figure. 19.

Throughput of the proposed model is analyzed using equation below.

$$Throughput = R.(1 - PEP)$$

where R corresponds to data rate. Results are described in Figure. 20. The results outperform with (anwar2020performance) and are comparable with (triwinarko2021phy) as described in Table 6. 5G NR was integrated with Spatial Multiplexing MIMO while keeping other DSRC specifications the same (dey2020modified). Convolution coding was used in the system. The performance of the 4*4 MIMO concatenated with 5G NR was analyzed using MMSE and ZF equalizers (dey2020modified). We have used for 4*4 MIMO system. According to (obi2021mimo), among Maximum Likelihood (ML) Estimator Zero Forcing (ZF) and Minimum Mean Square Error (MMSE), ML performance is optimal.

Figure. 21 and Figure. 22 depict PRR of both NLOS and LOS. Our proposed approach for channel modeling in VANET i.e MIMO-STBC can be adopted in V2X communication and IEEE 802.11bd. Researchers are considering inducing MIMO-STBC in current VANET communication systems as mentioned above.

CHALLENGES AND LIMITATIONS OF THE PROPOSED MODEL

In the proposed model, multiple antennas and other hardware systems are used, so hardware complexity is higher. Since mathematical algorithms are used in the design of the beamforming system, a cutting-edge, highly processing DSP chip is required. Beamforming systems cost more than non-beamforming systems because they use more hardware resources and more sophisticated DSP chips. The use of more resources results in a higher power requirement for beamforming systems. Consequently, the beamforming system's battery drains more quickly.

In some cases, Perfect Channel State Information (CSI) is considered at the receiver. Reed Solomon codes work well for M-ary modulations schemes than BPSK systems.

CONCLUSION

The future of VANET will be driven by mmWave communications. In this manuscript, a tractable model using STBC-RS is proposed for achieving ultra-reliability of 1- 10^{-5}. The closed-form approximations of BER using RS in the AWGN channel and Rayleigh fading are derived. The results show that the proposed model outmatches previous BER estimation approaches of RS and STBC in 5G VANET networks. On comparing the model with existing VANET communicating systems it can be concluded that the proposed model performance is better than IEEE 802.11bd. We recommend that for designing V2X architectures, MIMO-STBC along with RS coding provides more useful results, since low PEP is received. The designed model can also be employed in 802.11p as a physical layer enhancement technique.

This research work provides the guidelines for quantitating the BER and PER in error control coding and a road map to design various VANET architectures. In future work, RS error probability can be analyzed for more number of antennas. Further, a VANET channel model for V2X communication can be developed using large antenna array sizes.

LIST OF ABBREVIATIONS

304	ASE	Amplified Spontaneous Emission
305	ASTBC	Alamouti Space Time Block Coding
306	AT	Atmospheric Turbulence
307	BCH	Bose–Chaudhuri–Hocquenghem [C-ITS] Cooperative-Intelligent Transport System
308		communications
309	FEC	Forward Error Correction
310	GSM	Global System Mobile
311	ICC	Interchannel Crosstalk
312	LOS	Line of Sight
313	MAC	Medium Access Control
314	MIMO	Multi-Input Multi-Output
315	NGV	Next-Generation V2X
316		item [NOMA] Non-Orthogonal Multiple Access
317	OFDM	Orthogonal Frequency Division Multiplexing
318	PHY	Physical Layer
319	PER	Packet Error Rate
320	PRR	Packet Reception Ratio
321	3GPP	3rd Generation Partnership Project
322	16QAM	Quadrature Amplitude Modulation
323	RS	Reed Solomon
324	STBC	Space-Time-Block-Coding
325	SPM	Sub carrier-Power Modulation
326	VANET	Vehicular ad-Hoc Network
327	V2I	Vehicle to Infrastructure
328	V2X	Vehicle to Everything
329	V2V	Vehicle to Vehicle

LIST OF NOTATIONS AND DEFINITIONS

331	H_{ef}^{H}	conjugate transpose of H_{ef}
332	km/h	Kilo meter per hour
333	γ	Signal-to -Noise Ratio
334	ψ	far-zone phase difference between adjacent elements
335	θ	represents angle of arrival in beamforming
336	ϕ	represents angle of reflection
337	s	corresponds to periodicity of complex weight
338	N	transmitting antennas
339	d	equidistant spacing between elements
340	f_d	Doppler shift
341	v	Relative velocity
342	n	Coded bits

343 **REFERENCES**

344 **[1]** Lone, Faisal Rasheed and Puri, Arjun and Kumar, Sudesh. (2013). Performance comparison of Reed
345 Solomon code and BCH code over Rayleigh fading channel, International Journal of Computer
346 Applications, 71 , 0975 – 8887. https://doi.org/10.5120/12603-9397

347 **[2]** Yi, Zhao and Zou, Weixia. (2020). A novel NE-DFT channel estimation scheme
348 for millimeter-Wave massive MIMO vehicular communications , IEEE Access 8, 1-12.
349 DOI:10.1109/ACCESS.2020.2988666

350 **[3]** W. Shen, L. Dai, J. An, P. Fan, R. W. Heath. (2019). Channel estimation for Orthogonal Time
351 Frequency Space (OTFS) massive MIMO, IEEE Transactions on Signal Processing, 4204 - 4217.
352 https://doi.org/10.1109/TSP.2019.2919411

353 **[4]** Shajahan Kutty, Student Member, IEEE, Debarati Sen, Member, IEEE. (2015) Beamforming for
354 millimeter wave communications: an inclusive survey, IEEE Communications Surveys Tutorials", 18,
355 DOI: 10.1109/COMST.2015.2504600

356 **[5]** Abuqamar, Abdealrahman and Hamamreh, Jehad M and Abewa, Mohamedou. (2021). STBC-assisted
357 OFDM with subcarrier power modulation STBC-assisted OFDM with subcarrier power modulation,
358 RS Open Journal on Innovative Communication Technologies, 2. DOI: 10.46470/03d8ffbd.275ae770

359 **[6]** Zhao, Chunli and Yang, Fengfan and Waweru, Daniel Kariuki and Chen, Chen and Xu, Hongjun.
360 (2022). Optimized distributed generalized Reed-Solomon coding with space-time block coded spatial
361 modulation, Sensors, MDPI, 22. https://doi.org/10.3390/s22166305

362 **[7]** Arshee Ahmed, Haroon Rasheed and Madhusanka Liyanage. (2021). Millimeter-wave channel mod-
363 eling in a vehicular ad-hoc network using Bose–Chaudhuri–Hocquenghem (BCH) code, Electronics
364 MDPI, 10. https://doi.org/10.3390/electronics10090992

365 **[8]** Elsayed, Ebrahim E and Yousif, Bedir B and Singh, Mehtab. (2022). Performance enhancement of
366 hybrid fiber wavelength division multiplexing passive optical network FSO systems using M-ary
367 DPPM techniques under interchannel crosstalk and atmospheric turbulence, Optical and Quantum
368 Electronics, Springer, 54, 1-31. DOI: 10.1007/s11082-021-03485-8

369 **[9]** Ahmed, Ejaz and Gharavi, Hamid. (2018). Cooperative vehicular networking: A survey, IEEE
370 Transactions on Intelligent Transportation Systems. 19, 996–1014. DOI: 10.1109/TITS.2018.2795381

371 **[10]** Dey, Utpal Kumar and Akl, Robert and Chataut, Robin. (2020). High throughput vehicular communi-
372 cation using spatial multiplexing MIMO, 10th Annual Computing and Communication Workshop
373 and Conference (CCWC), IEEE Xplore. DOI:10.1109/CCWC47524.2020.9031225

374 **[11]** Zhang, Mengyuan and He, Shibo and Yang, Chaoqun and Chen, Jiming and Zhang, Junshan. (2020).
375 VANET-assisted interference mitigation for millimeter-wave automotive radar sensors, IEEE Network,
376 34, 238 - 245. DOI:10.1109/MNET.001.1900271

377 **[12]** Jagannath, Anu and Jagannath, Jithin and Drozd, Andrew. (2020). High rate-reliability beamformer
378 design for 2x2 MIMO-OFDM system under hostile jamming, International Conference on Computer,
379 Communication and Networks (ICCCN) IEEE. DOI: 10.1109/ICCCN49398.2020.9209635

380 **[13]** Ali Rashid, Dil Nawaz Hakro, Tanweer M Rizwan and Kamboh Amjad Ali. (2019). Simulation based
381 vehicle to vehicle and base station communication, International Conference on Information Science
382 and Communication Technology (ICISCT) IEEE. DOI:10.1109/CISCT.2019.8777411

383 **[14]** Zhang, Di and Liu, Yuanwei and Dai, Linglong and Bashir, Ali Kashif and Nallanathan, Arumugam
384 and Shim, Byonghyo. (2019). Performance analysis of FD-NOMA-based decentralized V2X system,
385 67, 5024-5036, IEEE Transactions on Communications. DOI: 10.1109/TCOMM.2019.2904499

386 **[15]** Santumon, SD and Sujatha, BR. (2012). Space-Time Block Coding (STBC) for wireless networks",
387 International Journal of Distributed and Parallel Systems, 3. DOI:10.5121/ijdps.2012.3419

388 **[16]** Ehsanfar, Shahab and Moessner, Klaus and Gizzini, Abdul Karim and Chafii, Marwa. (2022).
389 Performance comparison of IEEE 802.11 p, 802.11 bd-Draft and a unique-word-based PHY in
390 doubly-dispersive channels, booktitle IEEE Wireless Communications and Networking Conference
391 (WCNC), 1815–1820, IEEE. DOI: 10.1109/WCNC51071.2022.9771810

392 **[17]** Yousif, Bedir B and Elsayed, Ebrahim Eld and Alzalabani, Mahmoud M. (2019). Atmospheric
393 turbulence mitigation using spatial mode multiplexing and modified pulse position modulation in
394 hybrid RF/FSO orbital-angular-momentum multiplexed based on MIMO, Optics Communications
395 Elsevier, 436, 197-208. https://doi.org/10.1016/j.optcom.2018.12.034

396 **[18]** Z. R. M. Hajiyat, A. Sali, M. Mokhtar, and F. Hashim. (2019). Channel coding scheme for 5G mobile
397 communication system for short length message transmission, Wireless Personal Communications,

398   vol. 106, no. 2, pp. 377–400. https://doi.org/10.1007/s11277-019-06167-7

399 [19]   M. Indoonundon and T. Pawan Fowdur. (2021). Overview of the challenges and solutions for 5G
400   channel coding schemes, Journal of Information and Telecommunication, Taylor Francis, vol. 5, no.
401   4, pp. 460–483. https://doi.org/10.1080/24751839.2021.1954752

402 [20]   Bocharova, Irina and Kudryashov, Boris and Lyamin, Nikita and Frick, Erik and Rabi, Maben and
403   Vinel, Alexey. (2019). Low delay inter-packet coding in vehicular networks", Future Internet MDPI,
404   (11), DOI:10.3390/fi11100212

405 [21]   Mane, Pradeep B and Belsare, Madhavi H. (2020). Evaluation of the performance of a Reed
406   Solomon coded STBC MIMO system concatenated with MPSK and MQAM in different chan-
407   nels, International Journal of Sensors, Wireless Communications and Control, 10, 153-163, DOI:
408   10.2174/2213275912666190410151455

409 [22]   Hai, Han and Li, Caiyan and Li, Jun and Peng, Yuyang and Hou, Jia and Jiang, Xue-Qin. (2021).
410   Space-time block coded cooperative MIMO systems, MDPI, 21. https://doi.org/10.3390/s21010109

411 [23]   Youssefi, My Abdelkader, Mouhsen, Ahmed. (2020). Performance improvement for vehicular commu-
412   nications using Alamouti scheme with high mobility, Journal of Telecommunications and Information
413   Technology, 47-56. https://doi.org/10.26636/jtit.2020.140120

414 [24]   Triwinarko, Andy and Dayoub, Iyad and Cherkaoui, Soumaya. (2021). PHY layer enhance-
415   ments for next generation V2X communication", vehicular communications, Elsevier. DOI:
416   org/10.1016/j.vehcom.2021.100385

417 [25]   Ghafoor, Kayhan Zrar and Kong, Linghe and Zeadally, Sherali and Sadiq, Ali Safaa and Epiphan-
418   iou, Gregory and Hammoudeh, Mohammad and Bashir, Ali Kashif and Mumtaz, Shahid. (2020).
419   Millimeter-wave communication for internet of vehicles: Status, challenges, and perspectives. IEEE
420   Internet of Things Journal, 8525-8546. DOI: 10.1109/JIOT.2020.2992449

421 [26]   Schulz, Philipp and Matthe, Maximilian and Klessig, Henrik and Simsek, Meryem and Fet-
422   tweis, Gerhard and Ansari, Junaid and Ashraf, Shehzad Ali and Almeroth, Bjoern and Voigt,
423   Jens and Riedel, Ines. (2017). Latency critical IoT applications in 5G: Perspective on the design
424   of radio interface and network architecture, IEEE Communications Magazine, 55, 70-78. DOI:
425   10.1109/MCOM.2017.1600435CM

426 [27]   Stepanets, Irina and Fokin, Grigoriy. (2019). Beamforming signal processing performance analysis
427   for massive MIMO systems, internet of things, smart spaces, and next generation networks and
428   systems, International Conference on Next Generation Wired/Wireless Networking Conference on
429   Internet of Things and Smart Spaces Springer, 329-341. DOI:0.1007/978-3-030-30859-928

430 [28]   White and Reil. (2016). Millimeter-wave beamforming: antenna array design choices and characteri-
431   zation. Rohde-Schwarz-Ad. Com Journal. DOI: 10.1007/978-3-030-30859-928

432 [29]   Lucian Andrei. (2012). BER analysis of STBC codes for MIMO Rayleigh flat fading channel, Telfor
433   Journal, 78-82. https://scindeks.ceon.rs/article.aspx?artid=1821-32511202078Plang=en

434 [30]   Goldsmith, Andrea, "Wireless communications", Cambridge university press, 2005

435 [31]   Kumar, Preethi and Jayakumar, M. (2010). Evaluation and analysis of bit error rate due to propagation
436   mechanisms of millimeter waves in a QAM system", Proceedings of the 12th International Conference
437   on Networking, VLSI and Signal Processing, 177-181. ISBN: 978-960-474-162-5

438 [32]   I.S. Gradshteyn and I.M. Ryzhik,"Table of Integrals, Series, and Products", Elsevier Book, p25.

439 [33]   Al-Barrak, A., Al-Sherbaz, A., Kanakis, T., Crockett, R. (2017). Enhancing BER performance
440   limit of BCH and RS codes using multipath diversity. Computers, 6 (2), 21. Computers MDPI.
441   https://doi.org/10.3390/computers6020021

442 [34]   Performance analysis of Reed-Solomon codes concatenated with Convolutional codes over AWGN
443   channel. APTIKOM Journal on Computer Science and Information Technologies, 1 (1), 27–32. DOI:
444   10.11591/APTIKOM.J.CSIT.100

445 [35]   Tiwari, S., Hirwe, A., Dubey, R. (2013). BER performane of LDPC RS code in STBC - OFDM
446   system. Citeseer, vol 1. https://ijireeice.com/wp-content/uploads/2013/03/8-o-Sandeep-Tiwari-ber-
447   performance-fo-lpdc.pdf

448 [36]   Saleh Hasson. (2019). Improving communication reliability in vehicular networks using diversity
449   techniques. Journal of Computational and Theoretical Nanoscience, 16 (3), 838–844

450 [37]   Hamarsheh, Qadri and Daoud, Omar Rawhi and Al-Akaidi, Marwan and Damati, Ahlam. (2022).
451   Robust Vehicular Communications Using the Fast-Frequency-Hopping-OFDM Technology and the
452   MIMO Spatial Multiplexing, International Journal of Communication Networks and Information

Security (IJCNIS), . DOI: 10.17762/ijcnis.v14i1.5216

[38] Anwar Waqar, Franchi Norman and Fettweis Gerhard. (2019). Physical layer evaluation of V2X communications technologies: 5G NR-V2X, LTE-V2X, IEEE 802.11 bd, and IEEE 802.11p. IEEE 90th Vehicular Technology Conference (VTC2019-Fall). https://doi.org/10.1109/VTCFall.2019.8891313.

[39] Anwar, Waqar and Krause, Anton and Kumar, Atual and Franchi, Norman and Fettweis, Gerhard . (2020). Performance analysis of various waveforms and coding schemes in V2X communication scenarios, IEEE Wireless Communications and Networking Conference (WCNC). DOI: 10.1109/WCNC45663.2020.9120732

[40] Dey, Utpal Kumar, Akl, Robert, Chataut, Robin, Robaei and Mohammadreza. (2020). Modified PHY Layer for High Performance V2X Communication using 5G NR, IEEE Annual Ubiquitous Computing, Electronics & Mobile Communication Conference (UEMCON), 2020, 0137–0142, DOI: 10.1109/UEMCON51285.2020.9298144

[41] Obi, E and Sadiq, Bo and Zakariyya, Os and Theresa, A. (2021). MIMO detectors: A comprehensive performance analysis, Nigerian Journal of Technological Research, 2021, DOI: 10.4314/njtr.v16i3.4

[42] Abbas, Taimoor and Sjöberg, Katrin and Karedal, Johan and Tufvesson, Fredrik and others. (2015). A measurement based shadow fading model for vehicle-to-vehicle network simulations, International journal of antennas, Hindawi. DOI: 10.1155/2015/190607

[43] Va, Vutha and Shimizu, Takayuki and Bansal, Gaurav and Heath Jr, Robert W and others. (2016). Millimeter wave vehicular communications: A survey, Foundations and Trends® in Networking, 10, Now Publishers, Inc. DOI: 10.1561/1300000054

[44] Shah, AFM and Karabulut, Muhammet Ali and Ilhan, Haci and Tureli, Ufuk. (2022). Influence of channel fading and capture for performance evaluation in vehicular communications, TechRxiv. DOI: 10.36227/techrxiv.21726395.v1

[45] Jameel, Furqan and Haider, M Asif Ali and Butt, Aamir Aziz and others. (2017). Performance analysis of VANETs under Rayleigh, Rician, Nakagami-m and Weibull fading, International Conference on Communication, Computing and Digital Systems (C-CODE), 127-132 DOI: 10.1109/C-CODE.2017.7918915

[46] Giripunje, Lokesh M and Vidyarthi, Abhay and Shandilya, Shishir Kumar. (2022). Routing and Congestion in Vehicular Ad-Hoc Networks (VANET's): Characteristics, Challenges and Solutions, Advances in VLSI, Communication, and Signal Processing, 313–336. Springer. DOI: 10.1007/978-981-19-2631-0$_2$9